Lund University
Physics Department
Attosecond Physics

Master's Thesis

Implementation of adaptive optics into a femtosecond laser chain

Author:
Sandhra-Mirella Valdma

Supervisors:
Dr. Cord L. Arnold
Dr. Miguel Miranda

LUNDS UNIVERSITET

September 2015

LUND UNIVERSITY

Abstract

Faculty of Science
Physics Department

Master of Science

Implementation of adaptive optics into a femtosecond laser chain

by Sandhra-Mirella Valdma

Optical aberrations are the main cause for reduced focusability and low peak intensity in laser beams. All the applications that rely on high peak power and/or small focus spot size, loose efficiency when optical aberrations are present. They can be reduced by using specially shaped optical elements, but all aberrations cannot be avoided completely.

In this thesis we used a new approach for reducing aberrations in a femtosecond laser beam. Usually, aberrations have to be corrected by using a deformable mirror with large diameter to avoid damage to the mirror. When the beam is expanded the peak intensity is reduced and the aberrations can be corrected. Deformable optics is normally not used for femtosecond lasers with kHz repetition rate and mJ pulse energy, because the price for implementation is often too high. We used a small deformable mirror, developed for applications in microscopy, with custom made ultrafast coating in order to correct aberrations in the femtosecond laser. Prior embedding the deformable mirror into the laser chain, we investigated its properties with a HeNe laser and an uncompressed femtosecond laser beam. The aberrations and focusability of the laser beam were measured with a Shack-Hartmann wavefront sensor and a CCD camera. Finally, the deformable mirror was integrated into the laser chain to reduce aberrations.

We demonstrated the measurement and correction of optical aberrations in a femtosecond laser chain. The high-order aberrations introduced by the deformable mirror itself currently prevent from increasing the focused intensity. Nevertheless, the method we proposed is promising and should be further investigated.

Popular Science Article

A Mirror into a Thousand Pieces

Imagine if we could shape the light in any way we want with a mirror consisting of small mirrors. The ability to do so would improve and help develop laser-based applications, thus making the technology more widespread. Today we use lasers everywhere: medicine, industrial manufacturing, micro-drilling and fundamental research etc. These applications require high intensity that can be produced by femtosecond lasers. Such lasers have very short pulses and high intensity. Femtosecond lasers are complex and consist of many optical elements (lenses, mirrors etc.), which, due to their inherent imperfections, cause distortions in the laser beam. These distortions, also called aberrations, are unwanted because they reduce the the overall quality of the beam (Figure 1).

With passive optical elements, such as specially shaped lenses etc., we are able to reduce some of the aberrations. However to improve the quality of an unstable and distorted laser beam, we will need something smarter. A solution for that is adaptive optics.

One could think of an adaptive optics system as a human visual system. There is a sensor measuring the light (aberrations) — retina in the eye, a computer calculating the shifts to produce a sharp image — the brain, and a deforming element to change the incoming light accordingly — the eye lens with muscles. When the image is not sharp the shape of the lens will change until optimum image is produced on the retina. Usually an adaptive optics system consists of a deformable mirror, a wavefront sensor and a computer. Many small segments that can be moved up and down, thus creating a wanted shape for the mirror, make a deformable mirror. Upon reflection from this kind of mirror aberrations can be corrected and the overall beam quality improved.

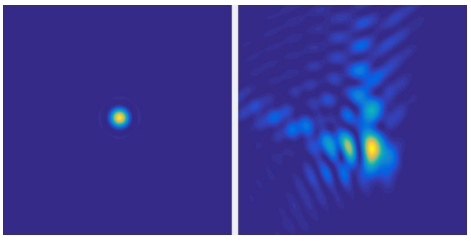

FIGURE 1: Optical aberrations cause larger and bubbly laser beam focus. Right: Ideal focus. Left: Focus of an aberrated beam.

These adaptive optics systems are usually very expensive for high intensity lasers. Usually the deformable mirror must have a large diameter to avoid damage from a high intensity laser beam. However, in this study we investigated a much cheaper option. We used a deformable mirror with a small diameter and a special coating and placed it in a femtosecond laser to correct aberrations.

We learned, that with this technique, it is possible to reduce aberrations in the femtosecond laser beam and although the resulting output was not ideal, it proved that the concept of using adaptive optics to correct high intensity femtosecond laser is solid.

Acknowledgements

Firstly, I would like to thank my supervisor Cord Arnold for his constant support and not giving up on me.

Secondly, I would like to thank all the members of Attosecond lab in the Lund University for creating a supportive and friendly environment for working. Especially, I would like to thank Antoine Jeandet for helping me finish my last measurements, Samuel Bengtsson and Esben Witting Larsen for explaining me the concepts of the femtosecond laser, and Karolina Dorozynska and Helene Coudert, who were always there, when I needed to talk.

Also, I would like to give my thanks for Thorlabs for enabling me to do this project by providing the custom made deformable mirror and Jürgen Hartmann for providing support with the user software.

Finally, I would like to thank Jan Bogdanov and my family for their constant support and encouragement throughout my studies.

This thesis was supported by Estonian national scholarship program Kristjan Jaak, which is funded and managed by Archimedes Foundation in collaboration with the Estonian Ministry of Education and Research.

Contents

Abbreviations

AO	**A**daptive **o**ptics
BS	**B**eam **s**plitter
CPA	**C**hirped **p**ulse **a**mplification
CW	**C**ontinuous **w**ave
DM	**D**eformable **m**irror
HeNe	**He**lium **ne**on
KD*P	potassium dideuterium phosphate
PSF	**P**oint **s**pread **f**unction
WFS	**W**ave**f**ront **s**ensor

Introduction

The laser, a pinnacle of modern technology, has, due to its uncountable high impact applications, been under constant development. A few decades ago, the first lasers with short pulses in femtosecond timescale ($10^{-15}s$), called femtosecond lasers, were built. Nowadays, femtosecond lasers are, because of the high light intensity they produce, widely used in the life sciences, industrial manufacturing, fundamental research, nano-structuring, micro-drilling of materials, femtosecond chemistry, attosecond physics and medicine. In order to achieve that high intensity the laser pulses must be focused down to a small spot size. However, femtosecond lasers often have low focusability due to the large amount of optical components they are comprised of. Imperfect optical elements produce wavefront distortions that should not occur in an ideal case. Some types of the aberrations can be avoided using specific optical elements, but not all. This creates the need for overall wavefront correction.

The solution for wavefront deformation is adaptive optics, i.e. optical elements, which can change their shape. The adaptive optics setup usually consists of detector for measuring the aberrations and deformable mirror for wavefront correction. Deformable mirrors consist of a reflective surface, whose shape can be changed by moving actuators connected from the back. Previously measured wavefront aberrations can thus be corrected upon reflection from that mirror.

Aim of the thesis

The objective of this master's thesis is to apply adaptive optics into a high average power femtosecond laser system in order to increase the laser's focusability. This in turn enables us to increase the efficiency of applications relying on high focal intensity.

Because of the complicated amplification process, the femtosecond laser chain contains many optical elements. In order to amplify the pulses and avoid damaging the laser itself, chirped pulse amplification (CPA) is used [1]. Before amplification the weak seed pulses have to be stretched in time to avoid damage during amplification stages. After amplification the femtosecond pulses are re-compressed close to their original duration. Due to the numerous wavefront distortions originating from the large number of optical components in the laser chain, the focusability and the peak intensity of the laser beam is reduced. A commercial adaptive optics solutions, i.e. sensor and mirror, can cost up to hundred thousand euros, a significant function ($20 - 25\%$) of the price of a femtosecond laser itself. The price is due to the large mirrors used in order to reduce the risk of damage by the high intensity beam.

In this thesis, we will use a deformable mirror developed by the optics vendor Thorlabs. This was originally developed for usage in microscopy. These deformable mirrors have a small diameter (10 mm) because the low peak intensities in these applications would not pose a threat to the mirror. This kind of adaptive optics set, together with wavefront sensor, costs less than 10000 euros. Our ambition is to integrate such a deformable mirror into a common femtosecond laser system with $1 - 10$ W average power, 100 Hz – 10 kHz repetition rate, 1 – 10 mJ pulse energy, and $20 - 100$ fs pulse duration. This has not been done yet with a small deformable mirror that has a silver coating, because the high intensity in the femtosecond laser could damage or deform the mirror surface.

For this thesis Thorlabs has modified the deformable mirror with a custom-made ultrafast coating. This means that due to low absorption of the highly reflective coating the high intensity beams do not damage the surface of the deformable mirror. To reduce the risk of damage even more, we will place the deformable mirror in the femtosecond laser chain before the compressor, where the pulses are still long in time and thus have lower peak intensity.

In addition to being a significant performance enhancement to the laser, implementing adaptive optics in this manner would, due to its reduced cost, lead to a more rapid spread of the technology in the ultrafast community.

Overview of the thesis

This thesis is divided into three main chapters. Chapter 1 presents a theoretical background of adaptive optics. The chapter is divided into sections regarding optical aberrations, Zernike polynomials, laser beam quality and overview of wavefront correction with adaptive optics. The femtosecond laser in the Lund Univeristy Atosecond laboratory, the Thorlabs deformable mirror and the Thorlabs wavefront sensor are described in chapter 2. Additionally, an overview of the optical setups used for wavefront correction is provided. The experimental part of this thesis is divided into three phases. In the first setup we used a helium-neon laser, which allows us to study the properties of the wavefront sensor and the deformable mirror under safe conditions. The output of this laser is almost perfectly Gaussian with very little abberations. Abberations can, however, be easily generated by e.g. deliberately misaligning optical components. In the next setup, a beam before the compressor in the femtosecond laser chain is directed out and used for measurements. This is done to see if the deformable mirror can be used to reduce aberrations in this specific laser beam without having to modify the laser chain. Chapter 3 presents the results and discussion based on the measurements. Finally, the thesis ends with the conclusion and the outlook of the project.

1 Overview of the field

In this chapter necessary background knowledge is provided. The chapter starts with introducing the optical aberrations that could affect the wavefront propagating through an optical setup. The first section presents a short overview of some of the most common optical aberrations. Subsequently, the Zernike polynomials are explained as the mathematical description of the optical aberrations. Following that, the point-spread function is introduced to show the effect of the aberrations on a point source. The aberrations introduce a need to estimate a laser beam quality which in this chapter is based on a method suggested by Siegman [2]. The last section introduces adaptive optics as a way to decrease wavefront aberrations. The most important elements in the adaptive optics are deformable mirrors (DM), which are also described in this section. A more detailed overview of a specific DM and a WFS used in this thesis is provided in Chapter 2.

1.1 Aberrations

Optical aberrations are wavefront distortions that deviate from ideal wavefront propagation. The phase $\phi(\vec{r})$ describes the wavefront and its aberrations. They usually occur due to imperfections of the optical system and/or the environment. Aberrations decrease the system's performance like focusability, resolution and intensity.

There are two main types of aberrations: monochromatic and chromatic. Monochromatic aberrations are mainly caused by the shape of optical elements and thus affect all the wavelengths the same way. Chromatic aberrations are caused by the dispersion of optical elements. It causes rays of different wavelengths to converge in different points in space. The most common monochromatic aberrations are spherical aberration, coma and astigmatism. In addition, piston and tilt are used to characterise wavefront slope and phase.

Spherical aberration

Spherical aberration is one of the most known aberrations because it results from optical elements with spherical surfaces. The marginal rays, that have a large angle to the optical axis, travelling through a lens have a bigger refraction angle than the paraxial rays, that have a small angle to the optical axis, which means that an image from the point source formed by the marginal rays does not coincide with the image formed by the paraxial rays. This causes the point image to fade into a circle with a finite size. The distance between those images increases with increasing angle between the paraxial and the marginal rays. The simplest way to eliminate or reduce the spherical aberration would be to use optical

elements with changing radii of curvature. Those so called aspheric lenses exist but are relatively expensive. [3] [4] [5]

Coma

Coma is similar to spherical aberration because in this case the paraxial and the marginal rays also produce an image in different distances from the optical element. The difference consists of the fact that incoming rays are not parallel to the optical axis of the lens. Coma occurs only for the objects that are off the optical axis. The name coma comes from a comet like shape that this aberration produces. This comet like shape directs away from the optical axis and is produced by different size images created by the marginal and the paraxial rays. [4]

Astigmatism

Astigmatism is often caused by a lens that has different curvatures in different planes which produces different focuses for the rays travelling in perpendicular planes. This means that the rays in the meridional and the sagittal plane focus in different planes perpendicular to the optical axis. This makes the image to change from an ellipse in one direction to an ellipse in another direction depending on which focus is observed.

1.2 Zernike polynomials

Optical system performance can be conveniently analysed by Zernike polynomials, which are especially useful for their properties over a circular aperature. All classical circular optical aberrations can be mathematically described by Zernike polynomials, which are orthogonal over an unit circle. Zernike polynomials are described by the following equations

$$\left.\begin{aligned} Z_{evenj} &= \sqrt{2(n+1)}R_n^m(\rho)cos(m\theta) \\ Z_{oddj} &= \sqrt{2(n+1)}R_n^m(\rho)sin(m\theta) \end{aligned}\right\} \quad m \neq 0$$
$$Z_j = \sqrt{n+1}R_n^m(\rho) \quad m = 0 \tag{1.1}$$

where n and m are positive integers (including zero), ρ and θ are polar coordinates and

$$j = \frac{n(n+2)+m}{2} + 1 \tag{1.2}$$

$$R_n^m(\rho) = \sum_{s=0}^{\frac{n-m}{2}} \frac{(-1)^s(n-s)!}{s![\frac{n+m}{2}-s]![\frac{n-m}{2}-s]!}\rho^{n-2s}. \tag{1.3}$$

The index n is called the radial degree or the order of the polynomial and m the azimuthal frequency. They must satisfy $m \leq n$ and $n - m = even$. Commonly polynomial ordering

number index j is used instead of n and m for simplicity. First Zernike polynomials related to optical aberrations are shown in Table 1.1 and plotted with Matlab in Figure 1.

Mode (j)	Order (n)	Frequency (m)	Zernike polynomials	Name
1	0	0	1	Piston
2	1	-1	$\rho\sin(\theta)$	Tip y
3	1	1	$\rho\cos(\theta)$	Tilt x
4	2	-2	$\rho^2\sin(2\theta)$	Astigmatism $\pm 45°$
5	2	0	$2\rho^2 - 1$	Defocus
6	2	2	$\rho^2\cos(2\theta)$	Astigmatism $0/90°$
7	3	-3	$\rho^3\sin(3\theta)$	Trefoil y
8	3	-1	$3\rho^3\sin(\theta) - 2\rho\sin(\theta)$	Coma x
9	3	1	$3\rho^3\cos(\theta) - 2\rho\cos(\theta)$	Coma y
10	3	3	$\rho^3\cos(3\theta)$	Trefoil x
11	4	-4	$\rho^4\sin(4\theta)$	Tetrafoil y
12	4	-2	$4\rho^4\sin(2\theta) - 3\rho^2\sin(2\theta)$	Sec. Astigmatism y
13	4	0	$6\rho^4 - 6\rho^2 + 1$	Spherical aberration 3
14	4	2	$4\rho^4\cos(2\theta) - 3\rho^2\cos(2\theta)$	Sec. Astigmatism x
15	4	4	$\rho^4\cos(4\theta)$	Tetrafoil x

TABLE 1.1: Zernike polynomials correspond to specific aberrations. [6]

Different aberrations can be easily separated, because Zernike polynomials are orthogonal and enable mathematical decomposition to assign specific coefficients to different aberrations. This wavefront aberration function is described as

$$W(\rho,\theta) = \sum_{j=1}^{J} a_j Z_j(\rho,\theta), \tag{1.4}$$

where a_j is and expansion coefficient

$$a_j = \frac{1}{\pi}\int_0^1 \int_0^2 \pi W(\rho,\theta) Z_j(\rho,\theta)\rho d\rho d\theta \tag{1.5}$$

and where J is the maximum value of j (highest order aberration used for wavefront reconstruction). [7] [8] [9]

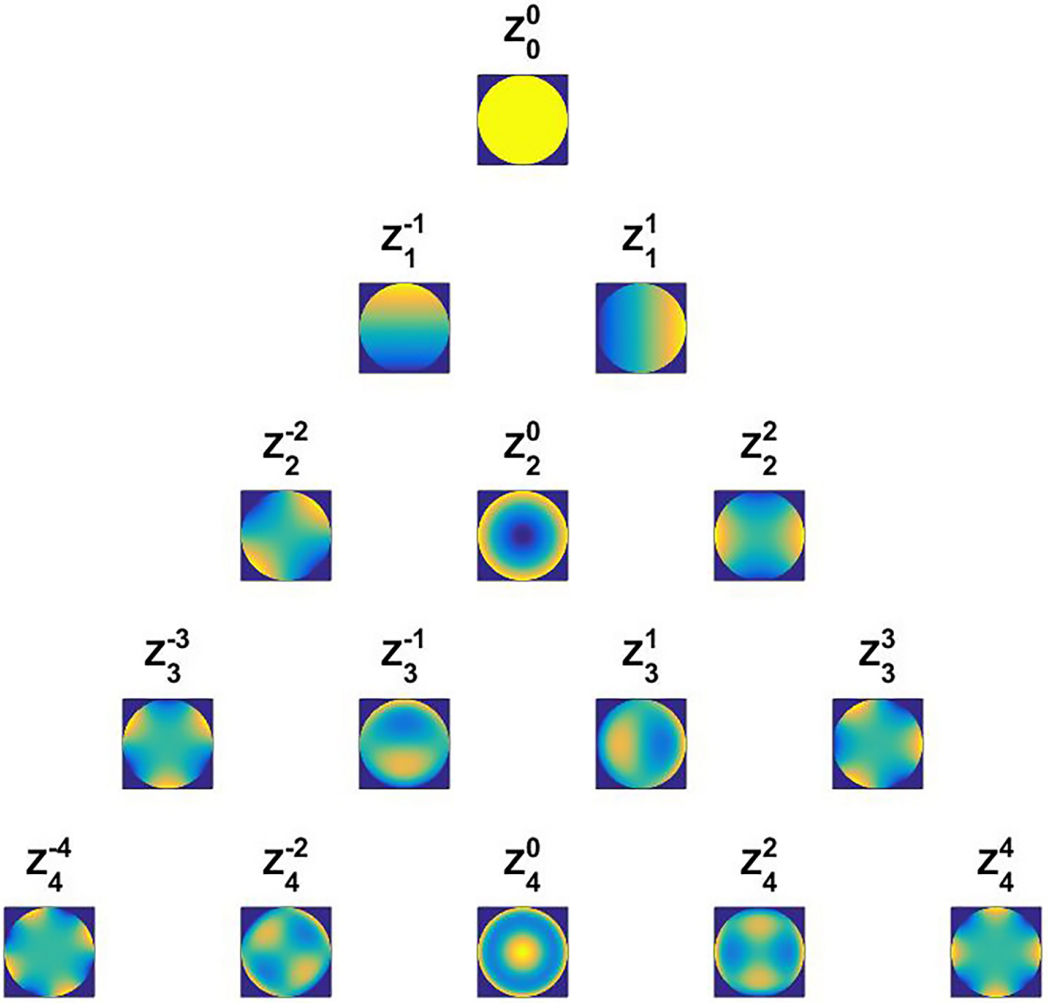

FIGURE 1.1: 15 first Zernike polynomials.

1.3 Point spread function

The point spread function (PSF) describes a diffraction image of a point source. It can be thought as an impulse response of the imaging system. In an ideal imaging system the PSF should also create a point image at the output, but in real life the output image is limited by diffraction and also affected by aberrations in the imaging system. Applying Zernike polynomials to the imaging system's PSF to model specific aberrations enables to see how different aberrations affect the image generation. PSF of imaging systems with aberrations corresponding to particular 15 first Zernike polynomials were plotted with Matlab (Figure 1.2).

$$PSF(\rho,\theta) = \frac{1}{\lambda^2 r^2 A^2} ||FT\left\{P(\rho,\theta)\cdot e^{-i\frac{2\pi}{\lambda}W(\rho,\theta)}\right\}||^2 \tag{1.6}$$

where λ is the wavelength, r pupil radius, A pupil area, FT Fourier transform, $P(\rho, \theta)$ the pupil function. [10] [11]

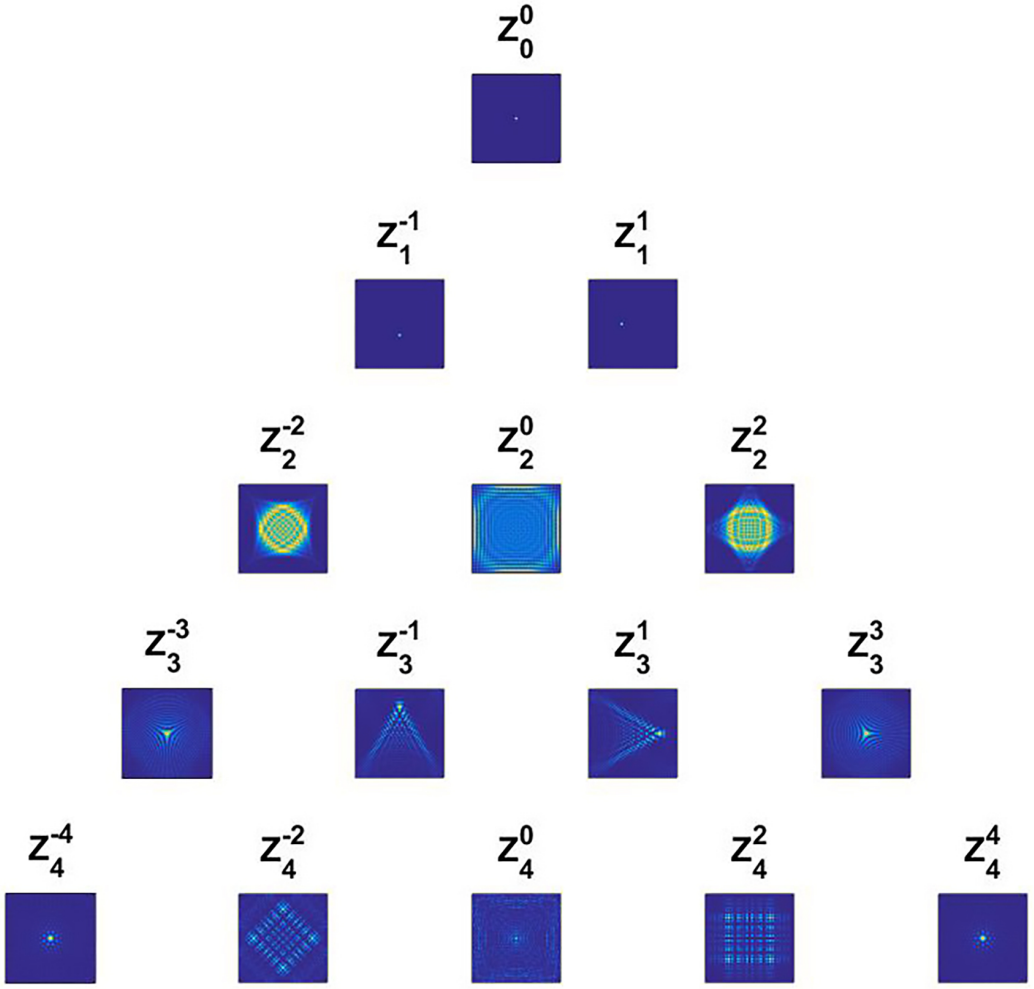

FIGURE 1.2: 15 first point spread functions of of imaging systems with aberrations corresponding to distinct Zernike polynomials.

1.4 Laser beam quality

In order to assess the laser beam's quality, information about the following parameters is required: M^2 factor, which describes the minimum spot size of a focused laser beam in relation to the focusing angle θ, W beam width and z_0 beam width location. M^2 factor and beam width location can be calculated by measuring the beam width around the focus. There are several different ways to measure beam width, for example: beam width measured from the first zero values of an image, variance of the intensity profile, width at $1/e$ or $1/e^2$ intensity points, the diameter contouring 86% of beam's energy etc. Those

definitions have different outcomes and are also not applicable to all beam profiles. Thus Siegman introduced in his article [2] a method based on second-order moments to specify the beam size.

Second-order moments can be easily calculated across both Cartesian coordinates. The following formulas are only provided for the x-direction because they are symmetric for the y-direction. The second-order moment across x is defined as:

$$\sigma_x^2 = \frac{\int_\infty^\infty (x - x_0)^2 \, I(x,y) \, dx \, dy}{\int_\infty^\infty I(x,y) \, dx \, dy}, \tag{1.7}$$

where $I(x, y)$ is the intensity at a specific point and x_0 is the centre of mass of the beam, which is defined as

$$x_0 = \frac{\int_\infty^\infty x \, I(x,y) \, dx \, dy}{\int_\infty^\infty I(x,y) \, dx \, dy}. \tag{1.8}$$

It can be shown that the beam diameter of a laser in the proximity of the geometrical focus can be described by the following equation:

$$\sigma_x^2(z) = \sigma_{x0}^2 + \sigma_\theta^2 \times (z - z_0)^2, \tag{1.9}$$

where σ_{x0} is the variance at beam waist, σ_θ is the variance of the angular spread and z_0 is the location of the beam waist. This quadratic form is independent from the actual transverse beam shape. Only restriction for using this form, is that the beam waist have to be measured using second-order moments.

For a Gaussian beam the spot size w_x in $I(x) = exp[-2x^2/w_x^2]$ is equal to twice the beam variance $W_x = 2\sigma_x$, where W_x describes the beam width based on the second-order moment. Even though W_x propagates the same way as w_x, the difference between w_x and W_x comes from usage of the M^2 factor. The second order moment beam width is expressed as:

$$W_x^2(z) = W_{x0}^2 + M_x^4 \times (\frac{\lambda}{\pi W_{x0}})^2 (z - z_{x0})^2, \tag{1.10}$$

where M_x^2 is a parameter describing beam quality. Thus laser beams can be characterized by six values: M_x^2, M_y^2, W_{x0}, W_{y0}, z_{x0} and z_{y0}. [2] Theoretically, laser beam can be ideally Gaussian with $M^2 = 1$, but for real lasers it is higher $M^2 > 1$. For example for HeNe lasers $M^2 < 1.1$ and for high intensity lasers it can be up to 4 [12]

1.5 Adaptive optics

Adaptive optics is an optical system, which is used to reduce wavefront aberrations. Adaptive optics is widely used in astronomy to reduce atmospheric turbulence, in microscopy and in retinal imaging. In the optical lab environment wavefront distortions are generally caused by optical elements. Adaptive optics is used to obtain the original shape

of the wavefront for being able to image an object without distortions or focus a laser beam to minimum spot size.

The most important components in a basic adaptive optics system are a deformable mirror (DM) and a wavefront sensor (WFS), which both are connected to a computer. This creates a system with a feedback loop (Figure 1.3). Incoming light will be sent to the DM from where it is reflected and directed to the WFS, where the wavefront distortion is measured and the gathered information is sent to the computer where the wavefront will be reconstructed. This information enables to calculate the specific shape for the DM, so that the wavefront aberrations can be corrected upon reflection from the mirror.

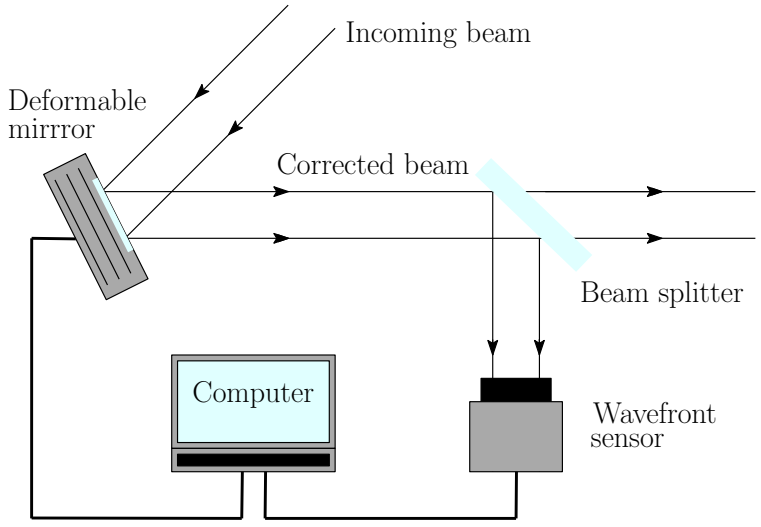

FIGURE 1.3: Common adaptive optics setup consists of a deformable mirror for wavefront correction and a wavefront sensor for wavefront sensing.

Mostly, the phase conjugation principle is used in adaptive optics systems. This means that an electric field's $Aexp(-i\phi)$ (amplitude A and phase ϕ) distortion will be compensated by adding the reversed phase. This means that reflection from a DM adds the complex conjugate of the initial electric field. The number of correction iterations depends on the dynamic of aberrations. Every time new wavefront data is collected and thus the shape of the DM can be corrected correspondingly. This makes it a closed loop system and thus allows for effective correction of the wavefront when abberations are changing over time. For adaptive optics system to work in such an environment it must do the measurement of the wavefront, calculations and change the shape of the mirror faster than the wavefront is changing. [13]

Deformable mirrors

DMs are mirrors whose shape of the reflective surface can be altered. This enables to correct the wavefront aberrations upon reflection. Usually they have many degrees

of freedom which makes them very useful in adaptive optics systems. Their reflective surface is connected to a number of actuators which enable to change it's shape. The actuators also determine how many numbers of freedom the mirror has. The precision of this kind of mirrors is reduced by the finite size of the actuator pitch (distance between actuator centres) and the stroke (maximum actuator displacement). Also the coupling will affect other actuators and can change their position incorrectly. In addition, the response time of the actuators is important, because if the wavefront is changing faster than the actuators can respond, the wavefront cannot be corrected.

There are many different types of DMs. All of them have their advantages and disadvantages. For example segmented DMs have only small cross-talk between actuators, but sharp edges of the segments cause scattering and diffraction. DMs with continuous membrane allow smooth wavefront control, but are affected by actuator coupling effects. MEMS (Microelectromechanical systems) based mirrors have fast response times, precision and low hysteresis. Also they can be quite inexpensve. DMs with reflective membrane consist of a small cross-section conductive and reflective membrane, which is controlled electrostatically by the actuators. Biomorph mirrors consist of two or more layers of different materials (with at least one piezoelectric or electrostrictive). The ferrofluid mirrors use small ferromagnetic nanoparticles that reside in a liquid and can be affected by an outside magnetic field. The shape of the mirror can be changed by the geometry of magnetic field. [13][14][15]

2 Methods

In this chapter we provide an overview of the components (Helium-Neon laser, femtosecond laser system, Thorlabs deformable mirror DMP40, Thorlabs wavefront sensor WFS10-5C) used in our experiments, a description of the DM and the WFS programs and explanations about the experimental setups we used at different stages in this thesis.

The aim of this thesis was to investigate the Thorlabs DM in femtosecond laser chain in order to correct optical aberrations in the laser beam. Even though, during the building of the laser chain, the presence of aberrations was attempted to be kept as low as possible, several optical elements together still cause noticeable optical aberrations. In order to examine and characterize the DM and the WFS, before entering the DM to the laser chain, we conducted our first measurements with a Helium-Neon (HeNe) laser. The beam of the HeNe laser is almost aberration-free, which makes it a good and controllable source. Firstly, we measured the wavefront (Zernike coefficients) with the Shack-Hartmann WFS and the focusability of the HeNe laser beam with a camera (Figure 2.1). Then we inserted the DM into the setup to investigate how it affects the wavefront. Also, we introduced abberations with an astigmatic mirror (AM). In order to correct them, we started the control loop program between the WFS and the DM.

Secondly, we took a reflection of the beam out from the femtosecond laser (Figure 2.2) and built a similar setup to measure wavefront and focusability. Those measurements were done to investigate the properties of the DM with a femtosecond laser beam that has low peak power and to avoid disrupting any ongoing research in the laboratory by building the DM into the laser chain.

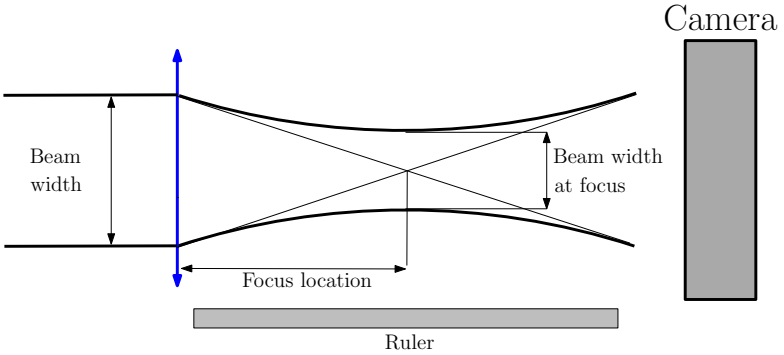

FIGURE 2.1: Beam width at different locations around the focus can be measured by moving the camera along the propagation direction.

Finally, we built a secondary path into the femtosecond laser chain before the compressor to check, if our main goal is achievable. Although we wanted to correct the output of the femtosecond laser of optical aberrations, we placed the DM before the compressor because the femtosecond pulses there are still long and thus the peak power of the pulses is much lower. Even though the DM is coated with special ultrafast coating, it could still be affected and damaged by the high peak power that femtosecond laser could produce. Since optical aberrations are linear the DM could be easily placed before the compressor and still correct optical aberrations that have accumulated in the laser chain.

2.1 HeNe Laser

Continuous wave (CW) helium-neon (HeNe) gas laser is very common in optics laboratories, because of its cheap price and nice Gaussian beam profile. Those lasers can be built to operate in either green, red or infrared. Usually they are constructed so that they their output beam is red at $632.8nm$. In this project we use the latter HeNe laser. Stimulated emission in HeNe gas lasers is achieved by pumping the gain medium, a mix of helium and neon gases, with an electrical discharge. Helium atoms need to be pumped into an excited state with no allowed radiative transitions. Then, those excited atoms transfer their energy to neon atoms through collisions. Neon atoms are transferred to metastable states, which enables stimulated emission to occur. Neon atoms have several energy levels below pump level, which means that there is more than one possible transition. [16] [17]

2.2 Femtosecond laser system

In this project we used 1 kHz femtosecond laser system at the Lund Attosecond Physcis laboratory (Figure 2.2). Since the laser system is being updated frequently the output parameters of the laser are not completely fixed. This laser system can produce 20 fs pulses with power of 5 mJ at 1 kHz repetition rate. The femtosecond laser pulses are centred around 800 nm and have 100 nm bandwidth. The system is based on chirped pulse amplification (CPA). CPA is used to generate pulses with higher pulse energy without damaging any of the optical components in the amplifiers. In this system short seed pulses are stretched temporally by introducing a large amount of dispersion. As a result different frequency components are resolved temporally and the pulse obtains a chirp. There can be two types of chirp: positive and negative. Frequency increases (decreases) with time with positive (negative) chirp. The stretching reduces the peak power of the pulses which makes them suitable for amplification stages. Subsequently, the pulses can be amplified to obtain higher peak power. Finally, the pulses are compressed by adding a negative (positive) chirp. The laser chain consists of a seed oscillator, Öffner type strecher, preamplifier, regenerative amplifier, 3-pass amplifier, cryo-cooled multi-pass amplifier and a compressor. The laser is described in detail in the coming subsections. The overview of the laser system is based on [18], [19] and [20].

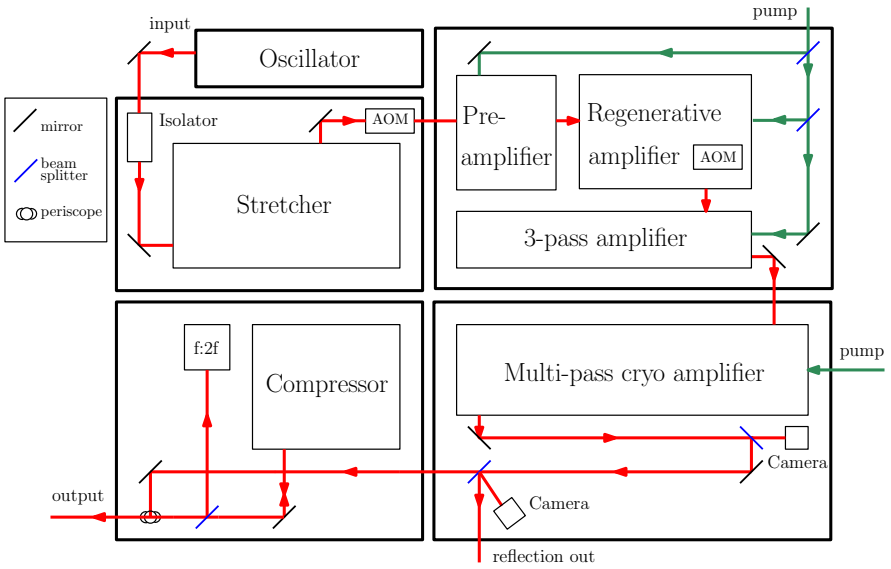

FIGURE 2.2: The femtosecond laser in Attosecond laboratory is based on chirped pulse amplification and can produce 20 fs pulses with an energy of 5 mJ.

The oscillator

The seed low energy femtosecond pulse to the laser system is provided by Femtolaser Rainbow oscillator. The oscillator uses a titanium doped sapphire (Ti:sapphire) crystal as a gain medium. The crystal has to be pumped by a frequency doubled CW neodymium-doped yttrium vanadate laser at 532 nm in order to produce stimulated emission.

This kind of oscillator favourably produces CW operation. Pulsed mode is achieved through mode-locking, which locks the phases of different spectral components. This generates a periodical pulse train. There are two main types of mode-locking: active and passive. The latter is used in this oscillator. The mode-locking is achieved in the oscillator by using the optical Kerr effect. This means that the refractive index of a material depends on an electric field applied to it by the laser beam. The refractive index of the Ti:Sapphire crystal is intensity dependent, which makes it a good choice also for mode-locking. The Gaussian pulse would cause the refractive index of the crystal to change so it would act as a gradient index medium (with highest refractive index at the centre). Together with an aperture after the crystal pulsed mode becomes more favourable than CW mode in the cavity.

The Femtolaser Rainbow oscillator produces 7 fs pulses at 800 nm central wavelength with a bandwidth of 200 nm. It has a repetition rate of 78 MHz and pulse energy of 2.5 nJ.

After the oscillator the beam is directed through an optical isolator. It allows the pulses to pass through, but prevents feedback from the laser chain. The optical isolator consists of a Faraday rotator that is placed in between two polarisers. A Faraday rotator is a

device, which rotates the polarization of incoming light. The rotation of the polarisation is independent of the direction of propagation. The polarisers are placed so that the beam entering the isolator is polarized linearly, the polarization is turned and the output polariser is placed under suitable angle so that the beam could pass through. However when the beam enters the isolator in the other direction the Faraday rotator turns the polarization so that it can not exit through the first polariser.

The stretching

After the oscillator, the pulse is directed through the isolator to the Öffner type stretcher (Figure 2.3). The stretching in CPA is required in order to decrease the pulse peak power through increasing the pulse duration before the amplification process. The pulse enters the stretcher under a retroreflector and is directed to a reflective diffraction grating. Subsequently, the beam passes through a mirror telescope and is reflected back to the grating. In this way the beam reflects from a grating twice per round trip (four all together) allowing it to produce positive group velocity dispersion (positive chirp). A pulse propagating through the optical elements in the laser chain usually gains a positive chirp. This results in pulse duration increasing to 400 ps. Finally, the beam is coupled out from the stretcher by a beam splitter and directed through a acousto-optical modulator (AOM).

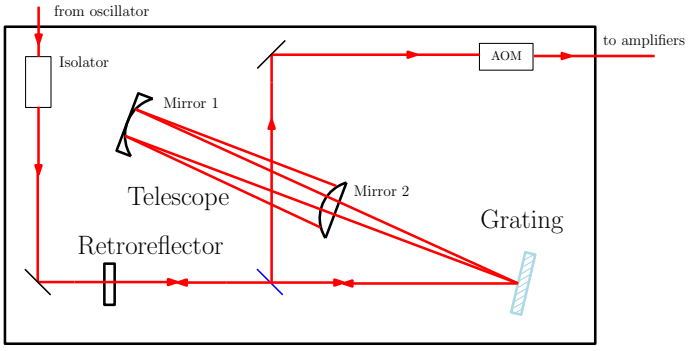

FIGURE 2.3: The Öffner type stretcher consists of a reflective diffraction grating and a mirror telescope, which enables a second pass. The stretcher adds a positive chirp to the pulse and increases the pulse duration up to 400 ps.

The amplification

Following the stretcher, the pulse is amplified in four different amplification stages. Firstly, it is sent to a preamplifier, from there to a regenerative amplifier, a 3-pass amplifier and finally, a cryo-cooled multipass amplifier. All the amplifiers use Ti:Sapphire crystals as gain medium. The crystals are pumped with to 30 W frequency doubled neodymium-doped yttrium lithium fluoride crystal lasers.

The pulse gains the energy of 250 nJ with 13 round trips in the preamplifier. Subsequently, a pulse picker is used to decrease the repetition rate to 1 kHz and directed to the regenerative amplifier. It consists of two potassium dideuterium phosphate (KD*P) Pockels cells. With 13 round trips the pulse has gained a saturation level with the energy of 0.5 mJ and can be directed out by one of the Pockels cells. Subsequently, the pulse goes through a 3-pass bow tie shaped amplifier, where it gains the energy of up to 3 mJ. Lastly, the pulse is amplified in the cryo-cooled multi-pass amplifier. With three passes the pulse can gain the energy up to 10 mJ. Usually, the pulse is amplified to around 7 mJ to reduce the damage risk for the optics. The last amplifier is cooled to cryogenic temperature ($-150°C$) to reduce the effect of thermal lensing, resulting from the heat gradient in a strongly pumped Ti:Sapphire crystal. Cryo-cooling is a common technique for high-average power femtosecond lasers. After the cryo-cooled amplifier, the beam alignment is checked with two aligned cameras. A reflection from one of the optical components is directed out from the laser chain and can be used for measurements.

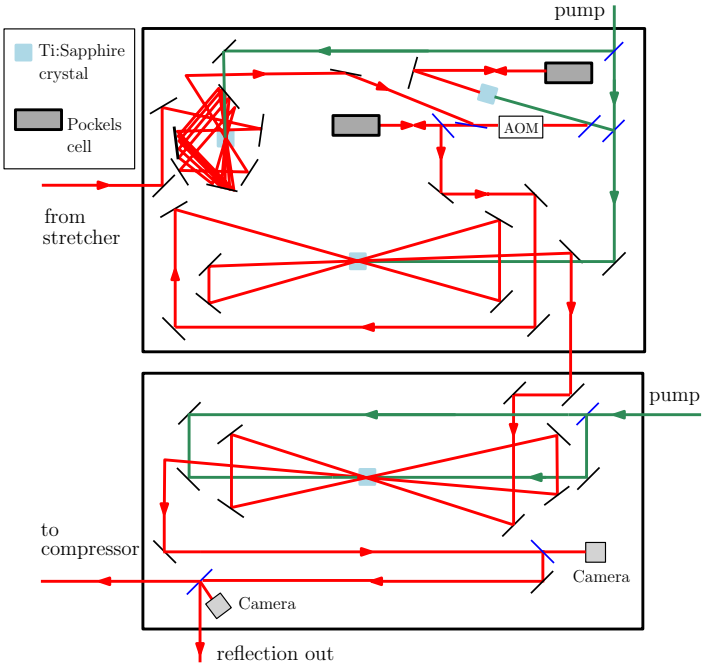

FIGURE 2.4: There are four amplification stages at the femtosecond laser chain: preamplifier, regenerative amplifier, 3-pass amplifier and cryo-cooled amplifier. The laser pulses can gain the energy up to 10 mJ.

The compression

The compressor is based on two reflective diffraction gratings and a retroreflector so that the positive chirp caused by the stretcher and other optical elements in the laser chain can be compensated with a negative chirp introduced by the grating compressor (Figure 2.5). Before sending the pulse to the compressor, the beam is expanded 10 times with

a telescope in order to decrease pulse power to prevent damage to the gratings. The gratings introduce a negative chirp and compress the pulse to a duration of around 20 fs with a maximum pulse energy of 5 mJ. The pulse is centred around 800 nm with a bandwidth of 100 nm.

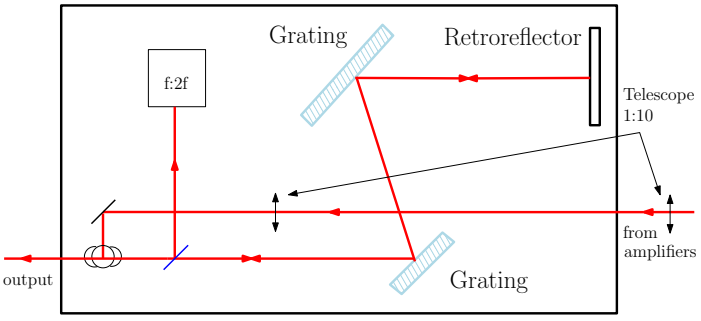

FIGURE 2.5: The pulse duration is compressed by a grating compressor to 20 fs.

2.3 Deformable mirror DMP40

The overview of the Thorlabs deformable mirror DMP40 and its user software is based on the Thorlabs manual [21]. The mirror has a diameter of 12.7 mm (together with sidearms) and a pupil of 10 mm (usable area).

The DM uses the piezoelectric effect to alter the shape of the mirror surface. The mirror consists of a a glass substrate, which is covered with a custom-made ultrafast coating. The glass substrate is glued on top of a segmented piezoelectric disc, which has 40 movable segments and three bending arms for tip-tilt control (Figure 2.7). All segments are connected to ground by one common electrode and each of them can be separately controlled with DC voltage from $0-200$ V by a specific electrode (Figure 2.6). The surface of the piezoelectric segment is flat when 100 V is applied, is expanding with voltages below 100 V and is shrinking with voltages above 100 V. In this way the specific segment can locally have shapes form concave to convex.

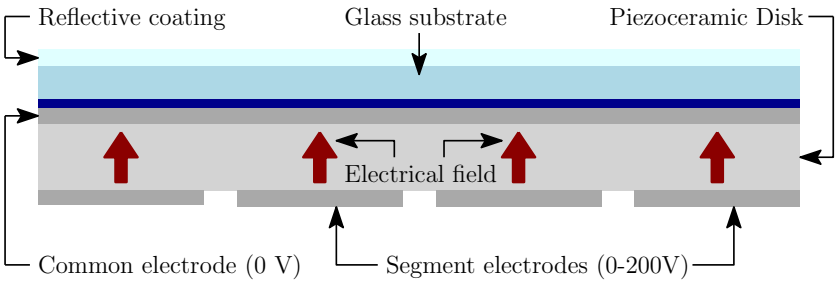

FIGURE 2.6: The shape of the deformable mirror can be changed by moving the segments. They can be controlled by applying a voltage to a specific segment.

The piezoelectric material used in the mirror suffers from hysteresis, which means that the mirror stroke is affected by the history of previous voltages that have been applied to a particular segment. Fortunately, Thorlabs has provided an automatic hysteresis correction in their software. The stroke is also affected by the creep effect, that is, a continuous material expansion of piezoelectric material after the voltage is applied. The creep is an ongoing process that never ends and logarithmically depends on time. It does not affect the beam properties in the closed loop setup, but without it, the creep will eventually cause the wavefront to drift. This means that piezoelectric mirrors cannot be used for holding a constant shape without feedback.

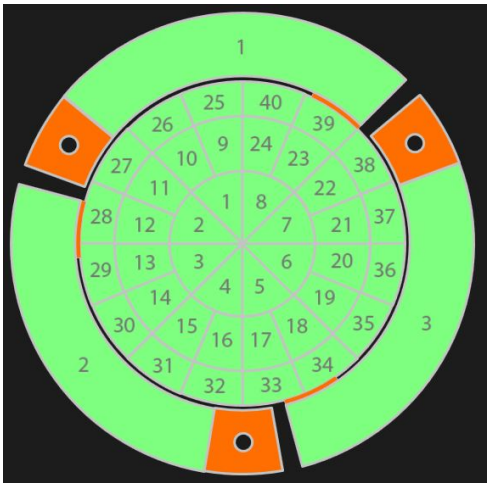

FIGURE 2.7: Thorlabs deformable mirror DMP40 mirror segments are placed in three circles for controlling the shape of the mirror. It also has three bending arms to control the angle of the mirror. (screenshot from the deformable mirror user software)

The Deformable mirror software

Thorlabs DM comes with ready-to-use software, which allows the use of a closed loop control. Together with the Thorlabs WFS, this enables to continuously correct wavefront aberrations. In this thesis we used a software ver. 2.2 provided by Thorlabs. The software enables basic mirror control. The user can save and load previously saved mirror segment voltage pattern, which defines the shape of the mirror. The software gives the opportunity to control the 15 first Zernike coefficients to produce mirror surface distortions that correspond to specific Zernike polynomials. The actuators are distributed in a way to reproduce Zernike polynomials with a good accuracy.

When the DM is connected to the computer, 100 V is applied to all the segments. Zernike coefficient sliders change the mirror shape so it would correspond to a specific Zernike polynomial. Also one can control each mirror segment separately by changing the segment voltages between $0-200$ V. Although the segment voltages can be saved, it is not possible to completely reproduce the shape of the mirror due to the hysteresis and the creep. The software takes the hysteresis into account when changing the shape of the mirror.

Also the creep and other mechanical tensions in the surface can be relaxed. It is done by continuously increasing and decreasing the voltages of all segments with a starting amplitude between $0 - 200$ V and decreasing it until the 100 V in the middle is reached.

Together with the Thorlabs WFS and its user software it is possible to establish a feedback loop between WFS and DM. Wavefront data is sent to the DM software which applies the calculated shape to the mirror so that the aberrations would be corrected upon reflection from the mirror. The software enables to choose which aberrations corresponding to the 15 first Zernike coefficients are corrected.

2.4 Shack-Hartmann wavefront sensor WFS10-5C

The overview of the Thorlabs Shack-Hartmann wavefront sensor WFS10-5C and its software is based on the Thorlabs manual [6]. The WFS consist of a microlens array, which is connected in front of a CMOS camera (Figure 2.8). All the lenses in the array have the same focal length hence, small sections of a beam filling the array are focused into small spots on the detector. The detector is placed in the focal plane of the lenslet array, and thus a spot diagram is created on the detector. Wavefront aberrations cause those spots to shift compared to the reference points (predefined centre points) and this shift enables to the wavefront direction locally at the position of a particular lens in the lenslet array. From the measurement of the local directions of the wavefront at the position of each lens, a map of the whole wavefront can be calculated.

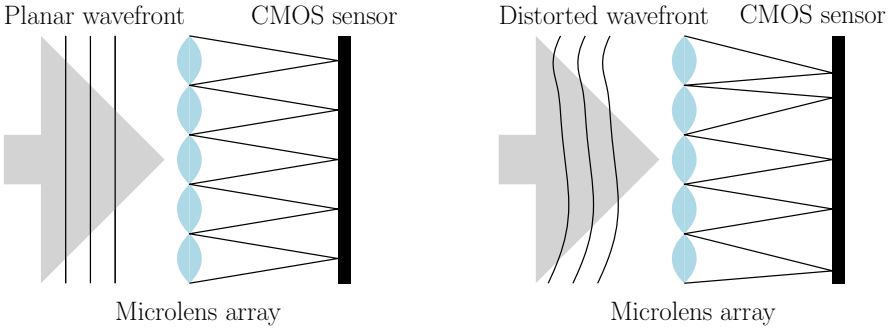

FIGURE 2.8: Wavefront sensing in the Shack-Harmann wavefront sensor is done with a microlens array and a sensor. The incoming light is focused by the microlens array generating a spotfield at the sensor. The wavefront aberrations can be calculated by measuring the spot shifts compared to planar wavefront spotfield.

The shifts can be calculated by subtracting the coordinates of the reference points from coordinates of the measured points. The spots are shifted in x and y direction and separated by an angle α. It can be shown that if the incoming wavefront enters under an angle α at this point then it is the same angle ($tan\alpha = \frac{\Delta z}{\Delta y} = \frac{\delta y}{f_{ML}}$). Also when the partial

derivation of the wavefront $W(x, y)$ is taken, it can be seen that it is dependent on the shift of the spots δx and δy and the focal length of the microlens array f_{ML}:

$$\frac{\partial}{\partial x}W(x,y) = \frac{\delta x}{f_{ML}} \qquad \frac{\partial}{\partial y}W(x,y) = \frac{\delta y}{f_{ML}} \tag{2.1}$$

The wavefront $W(x, y)$ is calculated when the spots' shifts are integrated. This is not a continuous method and thus there are discontinuous steps in the wavefront.

The Wavefront sensor software

In this thesis we used a software ver. 4.4 provided by Thorlabs to operate the WFS. The software measures the locations of the focal spots generated by the lenslet array and compares them to the internal reference or previously saved calibration file. From this shift the software calculates the Zernike coefficients and the wavefront. For best accuracy the beam size should be normally matched to the size of the lenslet array. The graphical interface of the software has five graph panels: lineview, spot field, beam view, wavefront, Zernike polynomials.

The lineview panel shows horizontal intensity distribution at the CMOS camera, where gray line shows the minimum pixel intensity and white line the maximum intensity. The power level at the camera can easily be checked with this graph. The pixel intensity can be changed by exposure time, master gain, black level and noise cut level.

The spot field panel shows measured image directly from the CMOS camera. Options like spots shifts, pupil and beam centre can also be shown on this graph.

The beam view panel shows beam intensity as a 2D plot. Although, due to the lenslet array in front of the sensor the resolution of the intensity plot is reduced. It can take the measurements only from the focused spots. All other regions are calculated with mean values and can be interpolated to generate a graph. This reduces the accuracy of the graph.

The wavefront panel shows a 3D model of the calculated wavefront. It can be either calculated directly or only taking into account desirable Zernike polynomials (reconstructed wavefront). The last graph shows the difference between the measured and the reconstructed wavefront.

In a last view the coefficients for all Zernike polynomials are displayed in a bar plot, providing a fast and convenient overview of what aberrations are present.

2.5 Setup 1: HeNe laser beam correction

We build this setup so we could learn about and test the DM and the WFS in a safe environment. This was also necessary to decouple the preparatory work from the ongoing

research activities at the femtosecond laser. The measurements with this setup are divided into four stages: HeNe laser beam, adding the DM to the setup, adding the astigmatic mirror (AM) to the setup and loop correction.

Stage 1: HeNe laser beam

In stage 1 we constructed a setup so we could measure the focusability and the wavefront aberrations of the HeNe laser (Figure 2.9).

In order to use the DM in the later stages of this setup, we had to expand the HeNe laser beam to a size suitable for the DM entrance pupil. We used a telescope with lenses $f_1 = 30$ mm and $f_2 = 200$ mm. Following that we directed the beam to a beam splitter (BS). One part of the beam went through a second telescope with lenses $f_3 = 150$ mm and $f_4 = 50$ mm to the WFS. It is important to notice that the adaptive optics system needs a 4f imaging system in order to work. The DM and the WFS need to be at the same plane. The DM must be 150 mm from the front of the telescope and the WFS 50 mm from the back of the telescope. The other part of the beam goes through a lens with $f_5 = 1000$ mm and is directed to a UEye camera. The camera can freely move back and forth along the beam's direction. This enables taking measurements of the beam width along the lens focus. The images were taken every 5 mm and enabled to plot the beam radius change along the propagation direction. From such setup e.g. astigmatism can easily be seen by eye, if the position of the foci in two perpendicualr directions (e.g. x- and y-directions) are not located at the same distance from the lens. Also we used Matlab script to calculate M^2 values for all the measurements to assess and compare the focusability.

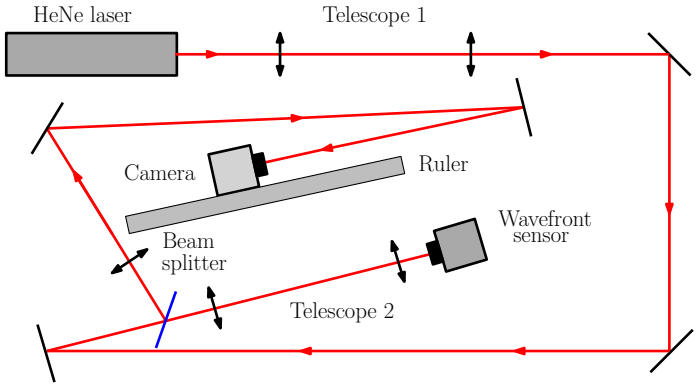

FIGURE 2.9: The setup to measure the wavefront and the focus of the HeNe laser with the WFS and the camera

Stage 2: Adding the deformable mirror to the setup

In stage 2 we replaced a mirror in the setup before the telescope 2 with the DM (Figure 2.10) to learn more about the capabilities of the DM. In order to produce the flattest

wavefront possible, the loop program was started. As in the previous stage, we measured the wavefront with the WFS and the M^2 factor. This gave us an overview of the magnitude of aberration the DM would cause.

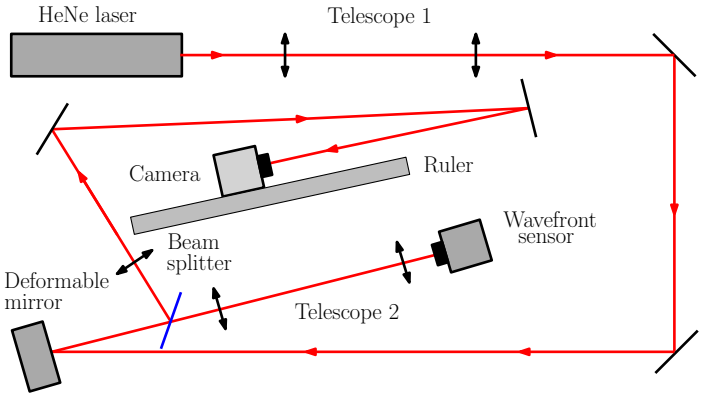

FIGURE 2.10: The setup to measure the DM effect on the HeNe laser beam.

Stage 3: Adding the astigmatic mirror to the setup

In stage 3 we used the AM to distinctively generate aberrations in the setup, which otherwise should be relatively aberration free. The AM was placed into the setup before the intended location of the DM (Figure 2.11). The astigmatic mirror (AM) is a small mechanical arrangement, in which a silver mirror can be bent by applying mechanical stress to it (Figure 2.12). While the mirror was connected to the holder with screws, it was slightly bent. Subsequently, the curvature of the mirror could be controlled by the connection screws and astigmatism was produced upon reflection from the mirror.

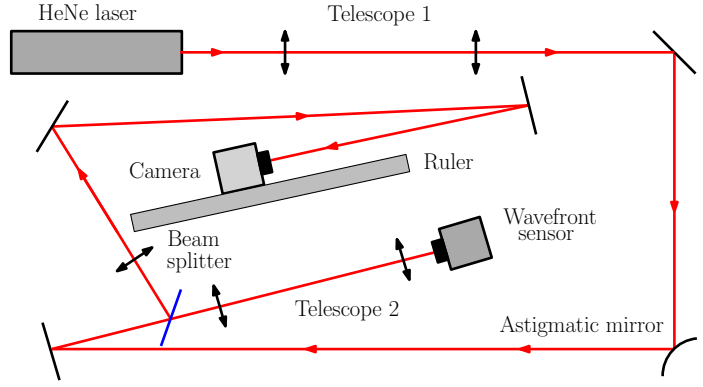

FIGURE 2.11: The setup to measure the astigmatic mirror effect on the HeNe laser beam

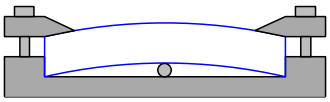

FIGURE 2.12: Astigmatic aberrations at the setup were achieved by using a mirror bent over a wire.

Stage 4: Loop correction

Finally, the DM was inserted again and the wavefront correction was enabled in the user software (Figure 2.13). This enabled us to see how this setup would affect the beam and how well would the DM correct the generated aberrations.

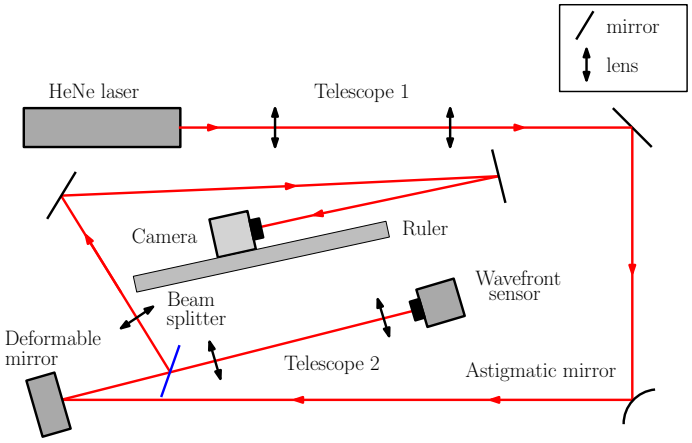

FIGURE 2.13: Setup used to investigate loop program and wavefront correction

2.6 Setup 2: Uncompressed femtosecond laser beam correction

The optical setup with the femtosecond laser beam was similar to the setup with the HeNe laser. The laser light was obtained from a weak reflection after the amplification stages (Figure 2.4). This meant that the laser could still be used by other researchers. This test had the purpose to investigate, if the ultrafast coating would work as intended and the WFS would be able to characterize aberrations, despite of the large bandwidth of 100 nm of the femtosecond laser.

Similarly to the setup with HeNe laser, the beam was first directed through an expanding telescope with a magnification of 3.33 and lenses $f_1 = 30$ mm, $f_2 = 100$ mm, in order to obtain suitable beam size for the DM and the WFS.

Stage 1: Uncompressed femtosecond laser beam

In stage 1 we built an identical setup as in setup 2, next to the femtosecond laser. At that point, the weak copy from the femtosecond laser had already passed through all the amplification stages, but was not compressed yet (Figure 2.4). We took the wavefront measurements with the WFS and investigated the focus with the camera (Figure 2.14).

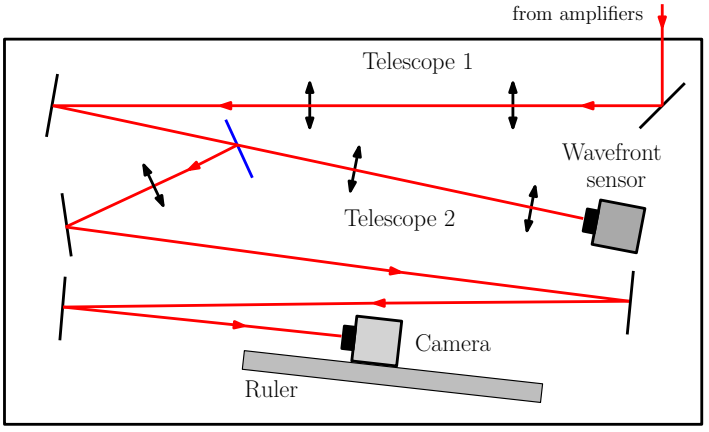

FIGURE 2.14: A setup to measure aberrations in the uncompressed femtosecond laser beam.

Stage 2: Adding the deformable mirror to the setup

In the second stage we replaced a mirror by the DM and took the same measurements with the flat DM to see how it would affect the wavefront of an already aberrated beam (Figure 2.15).

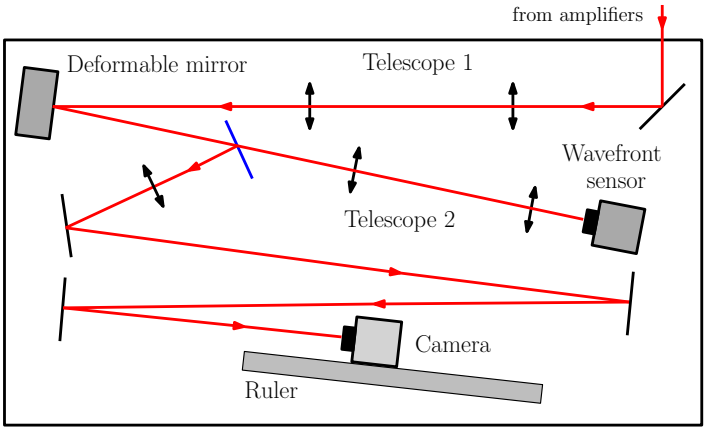

FIGURE 2.15: The setup with the deformable mirror enables to measure and correct aberrations in the laser beam

Stage 3: Loop correction

In the third stage we used the loop program between the WFS and the DM to correct the aberrations using the same setup.

Stage 4: Manual correction

Finally, we realized that sometimes manual correction might be more effective and thus stopped the loop program. We moved the Zernike coefficient sliders in the DM user interface to achieve the best focus shape at the position of the camera (geometrical focus).

2.7 Setup 3: Femtosecond laser beam correction

In this part we took two main measurements. Firstly, we measured the original laser beam without the DM in the laser chain to see which aberrations occur in the laser beam. Secondly, we looked at the shape of the focus at the camera and manually corrected the aberrations by using the Zernike coefficient sliders in the DM's user interface.

Stage 1: Femtosecond laser

In stage 1 of setup 3 we did not change anything in the femtosecond laser, however we built a small setup after the laser. It was the same as in previous section. We placed a lens with $f = 1000$ mm to focus a beam and took measurements with the camera. This was done so that we would be able to compare the measurement when we insert the DM to the compressor.

Stage 2: Manual correction

Final measurements were taken when the DM was placed inside the femtosecond laser chain right before the compressor (Figure 2.16). A second path through the compressor was built to place the DM into the chain. In this configuration the direct implementation of the WFS would have been complicated because identifying an identical plane to the position in the DM behind the compressor is not easy to achieve. The WFS was still used to measure aberrations at the output of the laser, but the feedback loop could not be closed in this configuration. Similarly, to a previous stage we measured the focus with the camera.

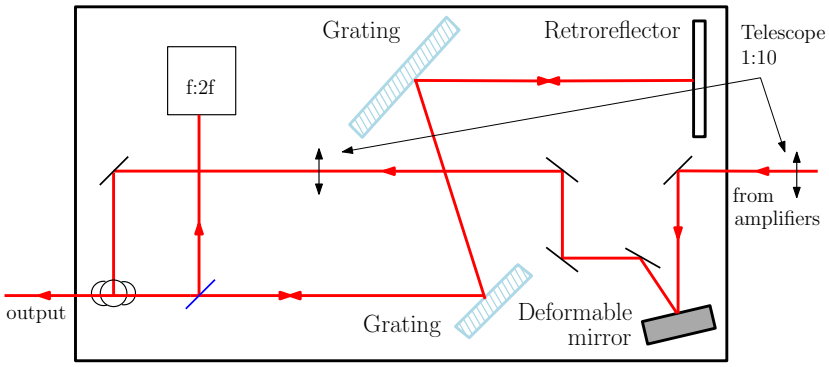

FIGURE 2.16: Placing the deformable mirror to femtosecond laser's compressor to correct aberrations at the output beam.

3 Results and Discussion

The measurements in this thesis were taken with setups described in the previous chapter. The results are also divided into the three measurements and their substages. Firstly, measurements with HeNe laser are discussed, secondly, an uncompressed output from the femtosecond laser chain was used for measurements and finally, the DM was implemented into the femtosecond laser chain. The beam width vs. propagation distance (caustics), which have been extracted from the camera images taken in the proximity of the geometrical focus, are shown for each case. We also fitted the results to a curve in order to calculate the M^2 factor, the minimum beam width W_0 and the location of the minimum beam width z_0. In addition, we plotted Zernike coefficient values of $4 - 15$ first Zernike polynomials for different stages of the measurements. It should be noted that the first three Zernike polynomials (offset, tip and tilt) have no influence on the focusability and were thus neglected. The plots give a good overview of the aberrations in the laser beam.

3.1 Measurements with setup 1: HeNe laser beam correction

Stage 1: HeNe laser beam

In stage 1 we built a setup to measure the quality of the HeNe laser beam with the WFS and the camera (Figure 2.9). As expected, the HeNe laser had an almost aberration free beam (Figure 3.1 and Figure 3.2). The flat wavefront indicates good focusability. The beam's foci for both directions almost coincide, indicating that the beam is not astigmatic (Figure 3.9). Unfortunately, we could not calculate M^2 values for measurements with the HeNe laser, because we did not go sufficiently far from the focus and thus could not fit the measurements satisfactorily enough.

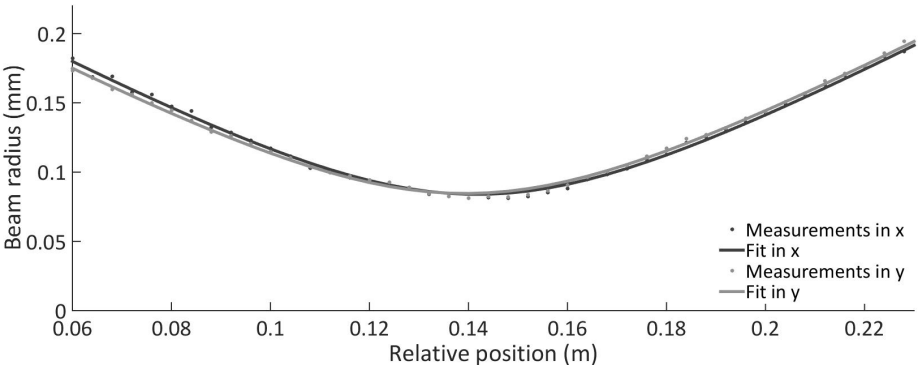

FIGURE 3.1: The graph shows that the HeNe laser has a good focusability with the focuses in x- and y-direction almost coinciding.

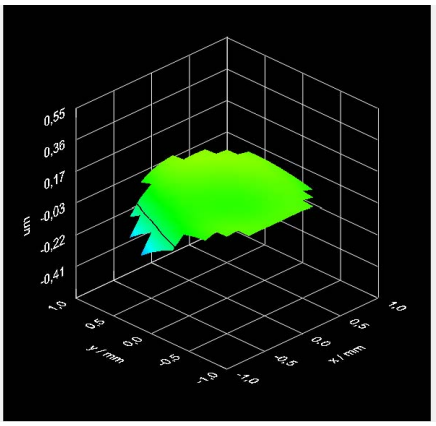

FIGURE 3.2: The reconstructed wavefront (15 first Zernike polynomials) of the HeNe laser beam

Stage 2: Adding the deformable mirror to the setup

In stage 2 we switched the third mirror in the setup to the DM in order to see how the DM affects the laser light (Figure 2.10). The loop program between the WFS and the DM was activated so that in ideal case the DM would produce flat wavefront upon reflection, but the feedback was not activated. Considering that the WFS measured only very small Zernike coefficients in the HeNe laser beam and the focusability was good, adding the DM to the setup definitely affected the beam quality considerably (Figure 3.3). The beam width increased and the foci in the x- and y-direction did not coincide (Figure 3.9). Even though the focusability was reduced considerably, the WFS still measured quite flat wavefront (Figure 3.4). We saw that the DM overcompensated a small tilt in the wavefront (Figure 3.2) by introducing too extensive opposite tilt (Figure 3.4). From this test can be concluded that having the DM implemented into an optical setup will increase aberrations and limit the intensity that can be achieved in the focus.

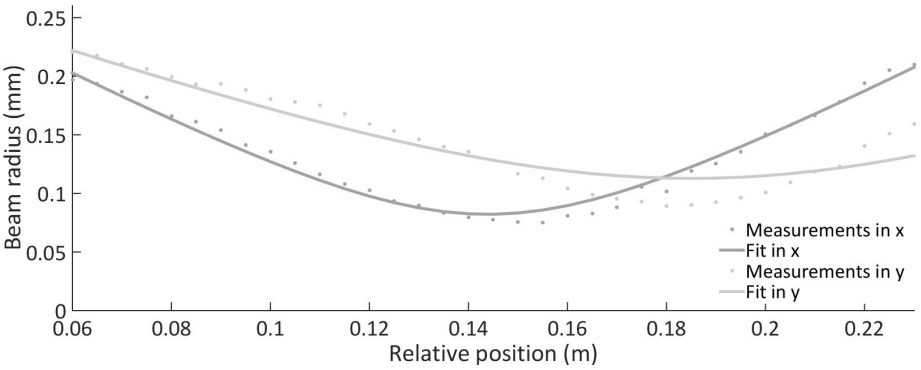

FIGURE 3.3: The focuses in x and y direction do not coincide, when the deformable mirror is inserted to the setup.

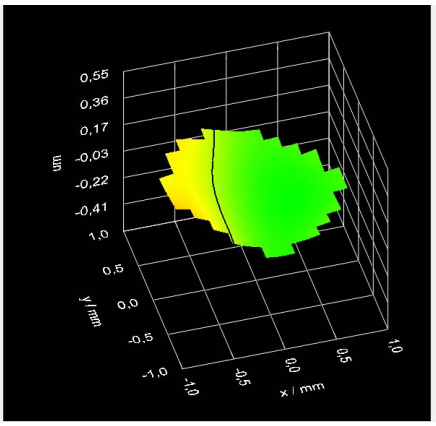

FIGURE 3.4: The reconstructed wavefront (15 first Zernike polynomials) of the HeNe laser beam with the deformable mirror inserted into the setup.

Stage 3: Adding the astigmatic mirror to the setup

In stage 3 we switched the second mirror in the setup to a astigmatic mirror (AM) to deliberately produce aberrations (Figure 2.11). By tightening the screws on the AM connections astigmatism could easily be introduced in the beam. As can be expected the Zernike coefficients increased with this setup. The AM had a really strong and predicted affect on the focuses in x- and y-direction (Figure 3.5). Also, the wavefront measurements show a strongly astigmatic wavefront (Figure 3.6). Surprisingly, the beam width did not increase noticeably compared to other previous measurements (Figure 3.1).

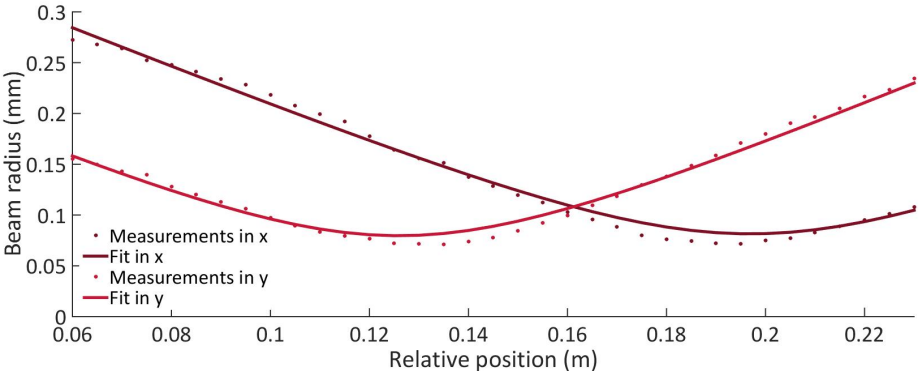

FIGURE 3.5: Rather nice astigmatism was achieved with inserting the astigmatic mirror into the setup

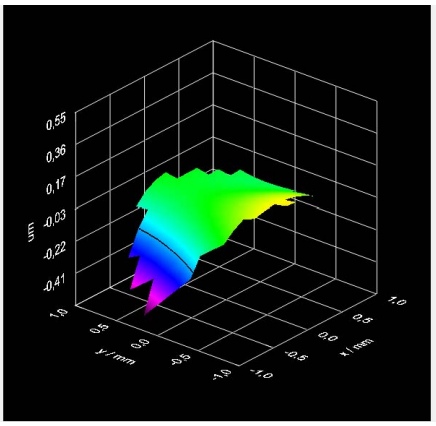

FIGURE 3.6: The reconstructed wavefront (15 first Zernike polynomials) of the HeNe laser beam with the astigmatic mirror inserted into the setup.

Stage 4: Loop correction

In stage 4 we had the AM and the DM both in the setup together and we started the loop program in order to correct the aberrations produced by the AM (Figure 2.13). As can be seen from Figure 3.7 the loop program corrected the aberration to some extent. The focuses in the x- and y-direction got closer but still had a small distance between them. The wavefront of the beam became more flattened but still had noticeable aberrations (Figure 3.8). The Zernike coefficient values were considerably reduced (Figure 3.9) with the loop.

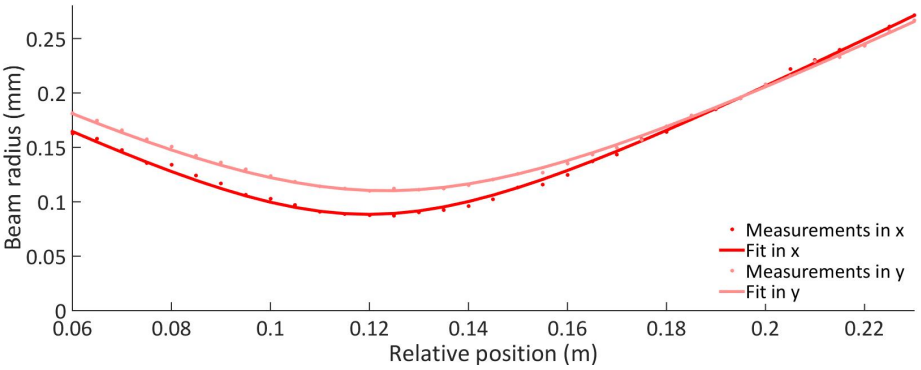

FIGURE 3.7: The loop program changed the shape of the deformable mirror so that the distance between the focuses in x- and y-direction decreased noticeably.

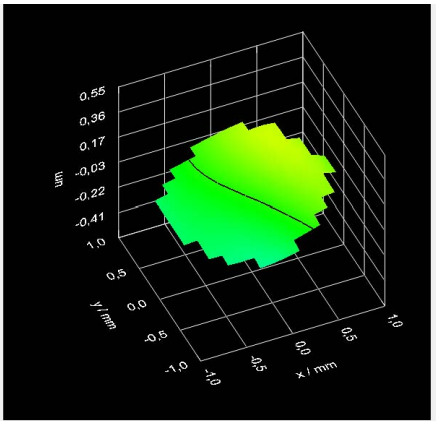

FIGURE 3.8: The reconstructed wavefront (15 first Zernike polynomials) of the HeNe laser beam with the loop control enabled to correct the astigmatic aberration.

Discussion of the measurements with the HeNe laser

In conclusion, the measurements with the HeNe laser, showed that it is possible to reduce astigmatism and other lower order aberrations with the DM and the loop program. As could be expected, the HeNe laser beam did not have any considerable aberrations in the beam. We saw that adding the DM to an already aberration free beam would increase the aberrations and in particular introduce astigmatism. However, the DM could significantly improve a strongly astigmatic wavefront (Figure 3.9). We used the focus measurement to calculate the beam width and z_0 the position of the focus. The beam width at the focus (W_x,W_y) increased with having the DM in the setup (Table 3.1). This was probably because the DM added significant higher order aberrations to the beam, which could not be corrected by the loop. We saw though, that the focuses in the x- and y-direction can be effectively closened by usage of the system. We could not compare the focus intensities between the different measurements, because replacing a mirror with the DM, decreased the intensity of the beam. This was caused by the lower reflection coefficient of the

ultrafast coating for the HeNe laser light. Overall, we saw that the adaptive optics setup reduced even significant aberrations, but did not eliminate the aberrations completely.

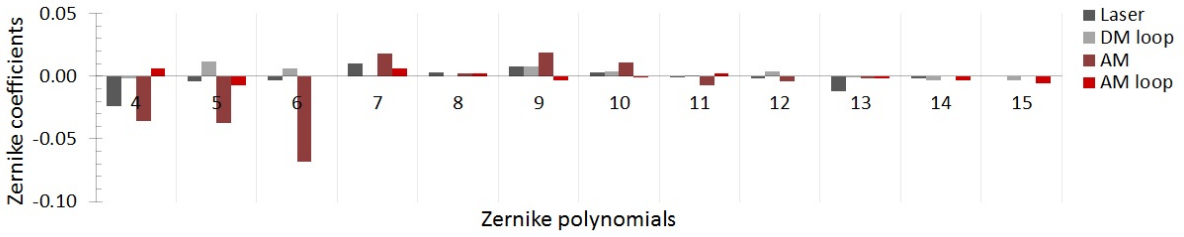

FIGURE 3.9: Zernike coefficient values for different measurement stages with the HeNe laser.

Measurement	W_x (mm)	W_y (mm)	z_{0x} (mm)	z_{0y} (mm)
HeNe only	0.08391	0.084566	141.676	139.3593
DM loop	0.08215	0.11279	143.8338	185.0051
AM only	0.081482	0.079649	196.9584	125.951
AM+DM loop	0.088442	0.11014	119.7206	123.38

TABLE 3.1: The beam width and the beam width location of the HeNe laser for the different measurement stages.

3.2 Measurements with setup 2: Uncompressed femtosecond laser beam correction

Stage 1: Uncompressed femtosecond laser beam

In the first stage we measured the uncompressed femtosecond laser wavefront aberrations with the WFS and its focusability with a camera. We saw that the beam's foci lie at different locations along the beam's travelling direction with having different beam widths for x- and y-direction (Figure 3.10). In addition, the M^2 factor values were rather high (Table 3.2). Partly, this could have been due to the fact that the fit was not the best or that the first telescope in the setup was not, due to its shortness, aligned precisely enough. The laser beam had considerable wavefront aberrations (Figure 3.11) and thus high Zernike coefficients (Figure 3.18). In the previous setup we saw that even when the reconstructed wavefront was quite flat in the WFS software, the focus of the beam still had aberrations. Therefore, here we also took images of the measured wavefront. It can be seen that there was a significant difference between the measured and the reconstructed wavefront. The measured wavefront graph was made directly from the measured data and the reconstructed wavefront was plotted taking into account the calculated 15 first Zernike coefficients. This showed that there were higher order aberrations in the beam.

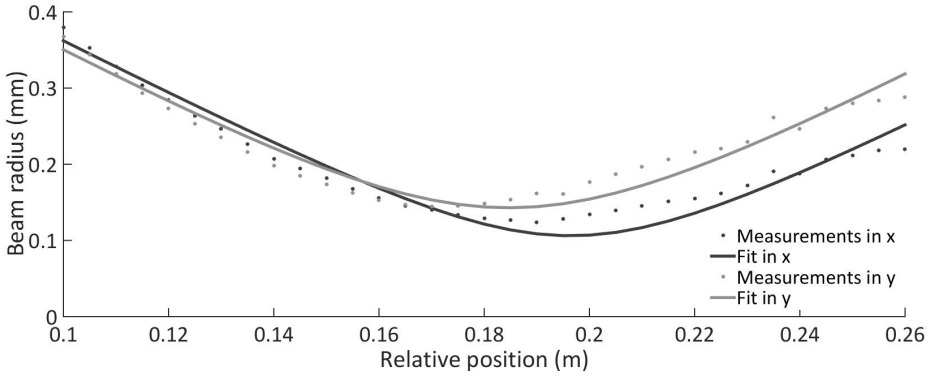

FIGURE 3.10: The graph shows that the uncompressed femtosecon laser beam has some aberrations, because the focuses in the x and y direction do not coincide and the beam width are also different.

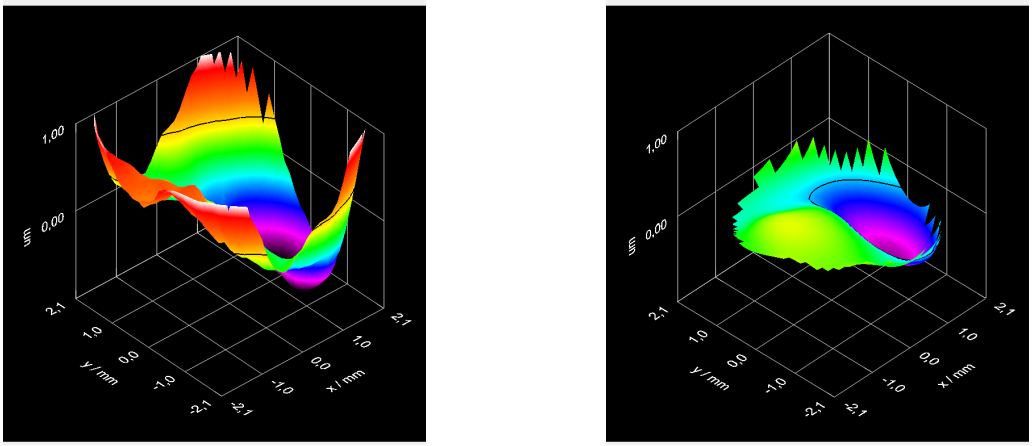

FIGURE 3.11: The measured (left) and the reconstructed wavefront (right) of the uncompressed femtosecond laser beam.

Stage 2: Adding the deformable mirror to the setup

In the second stage a mirror in the setup was changed to the DM (Figure 2.14). When the loop correction was not turned on, one could see that adding the DM caused considerable additional aberrations in the wavefront (Figure 3.13). The focusability of the beam was also reduced with increased distance between the focus locations in x- and y-direction (Figure 3.12). This was caused by the DM not having a completely flat surface, when turned on. The only way to produce a flat surface on the DM would be to calibrate the DM together with the WFS. The reference beam has to have a flat wavefront. Then, the DM and the WFS can be loop controlled so that the WFS shows smallest Zernike coefficients. The altered DM surface pattern has to be saved for later use. When this

pattern is used, the aberrations in the beam should look similar to the previous case where the DM was not yet inserted to the setup. Though, still it would increase the higher-order aberrations in the beam because of the segment edges and etc.

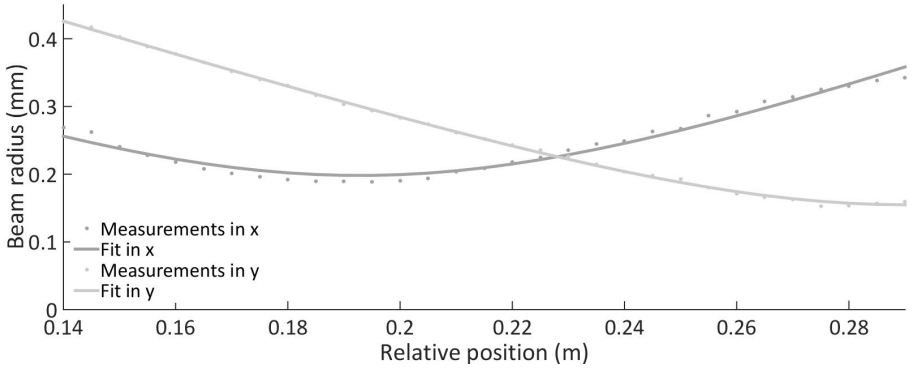

FIGURE 3.12: Similarly to measurements with HeNe laser and the deformable mirror the focuses of the beam in x- and y-direction do not coincide.

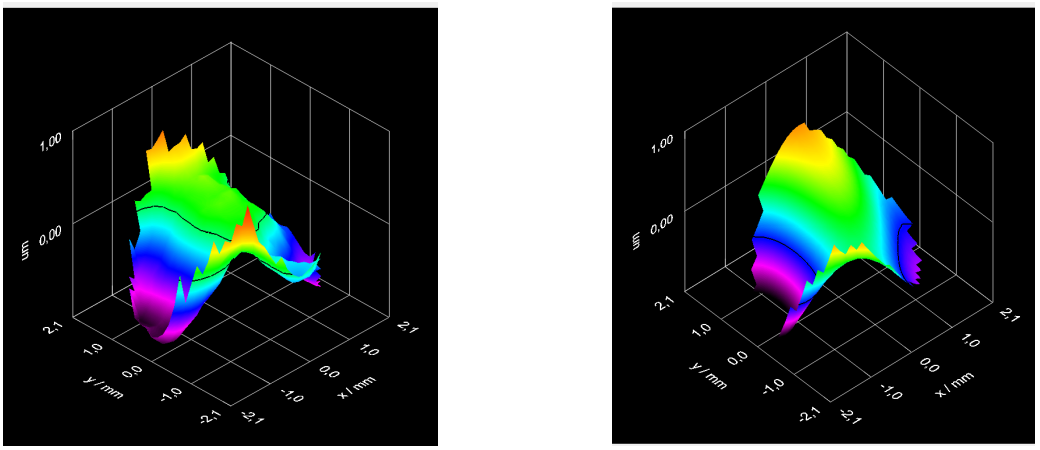

FIGURE 3.13: The measured (left) and the reconstructed wavefront (right) of the uncompressed femtosecond laser beam with the deformable mirror inserted into the setup.

Stage 3: Loop correction

In the third stage we started the loop program and let it run until we saw that the Zernike coefficient values at the WFS software were at their lowest values. We saw that even though the coefficients decreased, the focuses in different measurement directions were still separated (Figure 3.14). Clearly, the focusability increased and the aberrations

in the beam decreased when compared to the flattened DM measurements. Unfortunately, the loop did not improve the laser beam quality compared to the original beam measurements (Figure 3.10). We saw that the reconstructed wavefront was flat, but the measured wavefront showed strong higher-order aberrations (Figure 3.15). Since we saw that those fluctuations affected the wavefront significantly, we decided to manually fine adjust the DM shape provided by the loop. The next subsection gives an overview of those measurements.

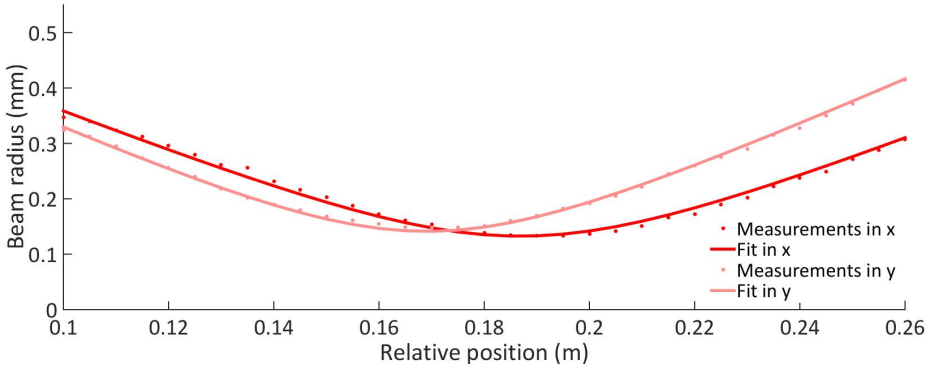

FIGURE 3.14: The loop reduced the aberrations in the laser beam so that the distance between the focuses in the x- and y-direction is reduced.

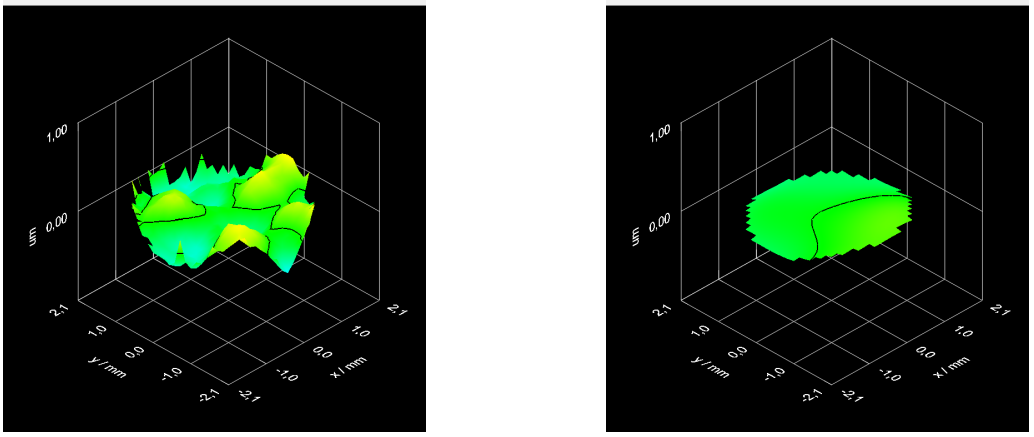

FIGURE 3.15: The measured (left) and the reconstructed wavefront (right) of the uncompressed femtosecond laser beam with the loop program activated.

Stage 4: Manual correction

In the forth stage we manually fine tuned the Zernike coefficient sliders and the mirror segments in the DM software to further decrease the aberrations in the beam. For reference we looked at the wavefront shape and the focal spot. This way we shifted the focuses in x- and y-direction much closer to each other (Figure 3.16). We could decrease

considerably the M^2 factor and the beam width in y-direction, but slightly increased them in x-direction (Table 3.2). We also saw that the higher order aberrations decreased in the measured wavefront (Figure 3.17).

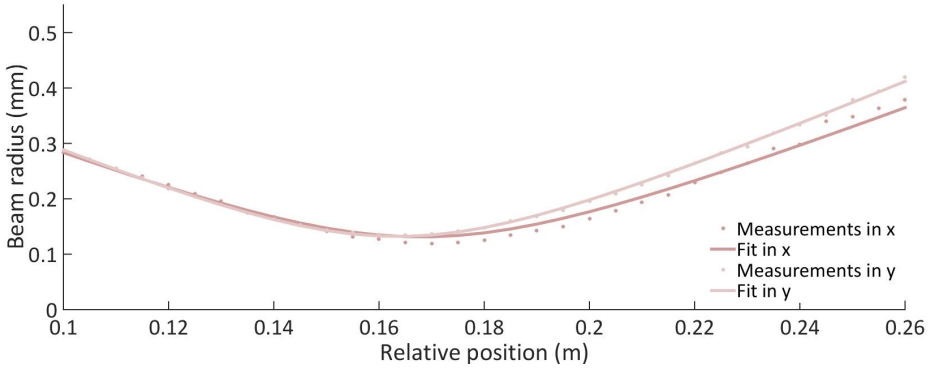

FIGURE 3.16: The distance between the focuses was decreased even further with the manual control of the deformable mirror

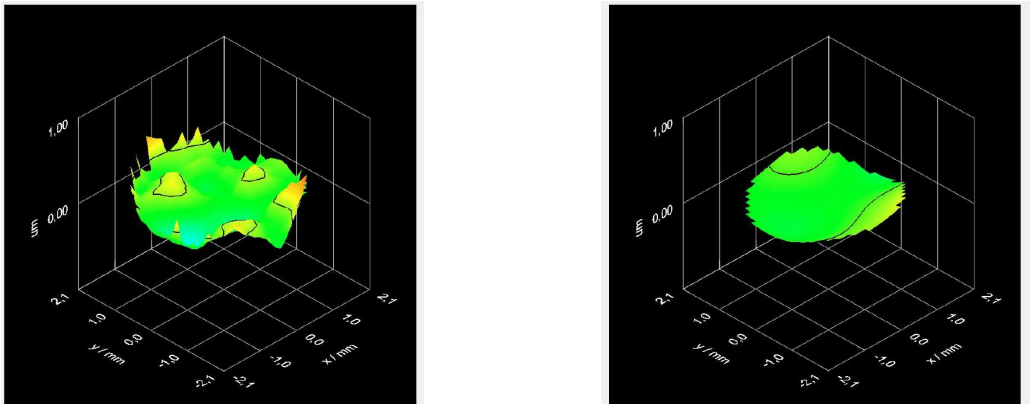

FIGURE 3.17: The measured (left) and the reconstructed wavefront (right) of the uncompressed femtosecond laser beam with manual correction of the aberrations.

Discussion of the measurements with the uncompressed femtosecond laser beam

In conclusion, the measurements with the uncompressed femtosecond laser beam showed that the lower order aberrations could be reduced. The uncompressed femtosecond laser beam had high astigmatism and small amounts of other aberrations (Figure 3.18) — this we also predicted previously. In those measurements, we saw, similarly to HeNe measurements, that adding the DM to the measurement setup would increase some of the lower order aberrations significantly. Therefore, the flattened DM would not be useful. The loop program, though, definitely decreased the aberrations in the uncompressed femtosecond beam. Still, the improvement would be insufficient when compared to the input beam's

quality (Figure 3.16) and Figure 3.10). We saw that the measured wavefront showed some fluctuations (Figure 3.15). Those fluctuations in the wavefront were probably caused by some of the mirror segments that had been moved slightly too much compared to other segments. We can reason that the loop program, which is not correcting higher order aberrations (Zernike polynomials over 15), causes the DM to overcompensate some of the segments, without affecting the lower order aberrations. Therefore, the DM shape was manually adjusted. We could improve the focus spot on the camera even though the WFS showed slight increase in the Zernike coefficient values (Figure 3.18). Also, we reduced the wavefront fluctuations (Figure 3.17). We saw that the beam width, the M^2 factor and the focus location could be easily controlled by the deformable mirror (Table 3.2). To summarise, the loop program could be improved to take into account the wavefront measurements more specifically and not to allow some of the DM segments overcompensate, thus generating higher order aberrations.

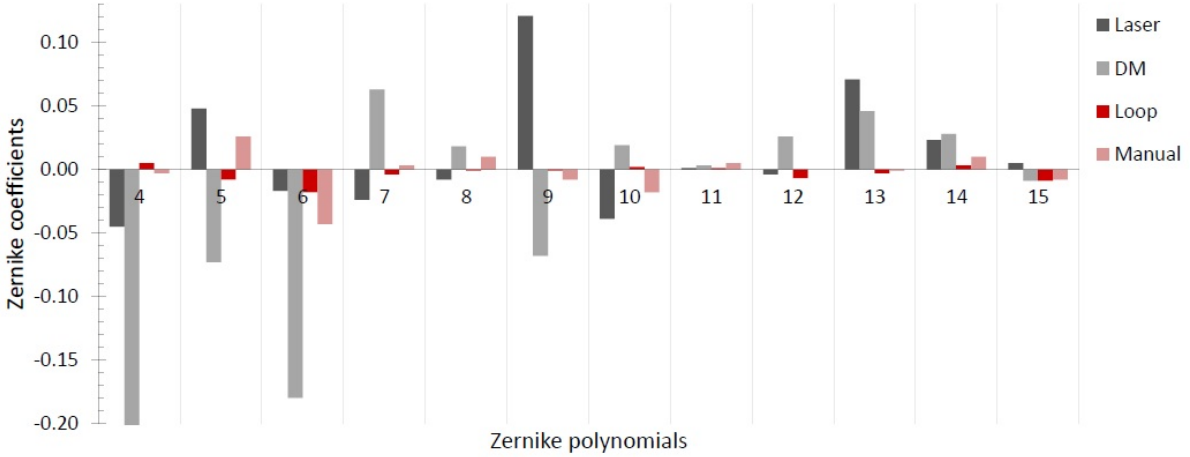

FIGURE 3.18: Zernike coefficient values of the measurements with uncompressed femtosecond laser beam.

Measurement	W_x (mm)	W_y (mm)	M_x^2	M_y^2	z_{0x} (mm)	z_{0y} (mm)
Laser only	0.110	0.145	1.93	2.71	196.1	183.5
DM	0.200	0.188	3.57	2.90	191.5	269.2
Loop	0.125	0.135	2.52	2.95	189.1	169.3
Manual	0.113	0.126	2.25	2.59	168.6	163.8

TABLE 3.2: Measurement results with the uncompressed femtosecond laser

3.3 Measurements with setup 3: Femtosecond laser beam correction

Stage 1: Femtosecond laser beam

The final measurements were done trying to improve the focusability and quality of the output beam of the femtosecond laser. Firstly, we took the focus measurements of the femtosecond laser beam without any modification of the laser chain (Figure 3.19). We could see that the beam has relatively good focusability, but the foci in x- and y-direction do not coincide (Table 3.3).

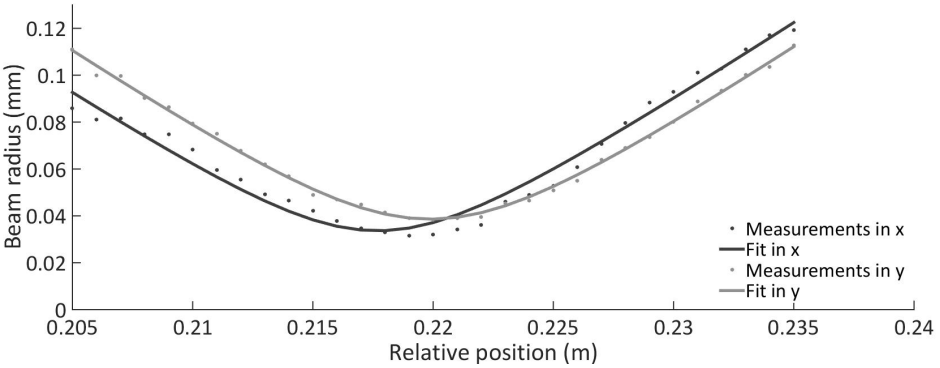

FIGURE 3.19: Femtosecond laser focuses in x- and y- direction did not coincide.

Stage 2: Manual correction

Secondly, we built a second path to the compressor and inserted the DM into the chain (Figure 2.16). This enabled us to control the beam shape before the compression in the femtosecond laser occurred. As mentioned before in section 2.7 we did not use the loop program because matching planes before and after the compressor is complicated. Also, in this part we controlled the DM shape manually by looking at the focus of the femtosecond laser beam.

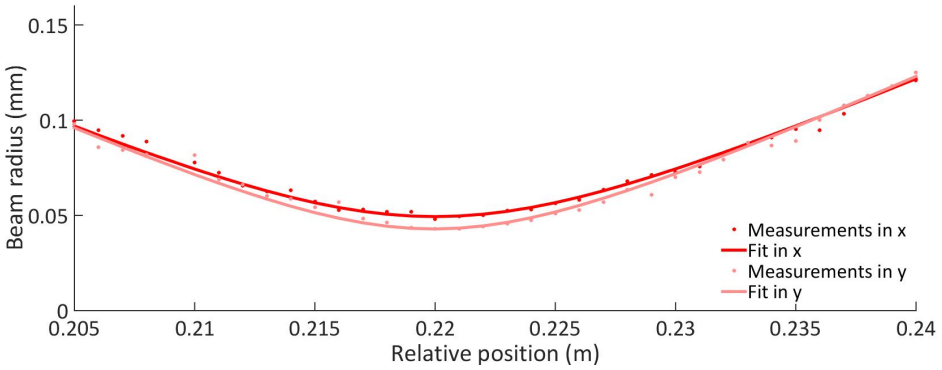

FIGURE 3.20: Astigmatism could be reduced compared to the original femtosecond beam when the deformable mirror was inserted into the laser chain and the aberrations were corrected manually.

Discussion of the measurements with the femtosecond laser

In conclusion, we saw that it is possible to use the DM in the femtosecond laser chain and slightly improve the focusability. We measured the focus of the femtosecond laser beam and saw that the foci in the x- and y-direction would not coincide. We reduced the distance between the foci by manually controlling the DM and looking at the focus measured with the camera (Figure 3.20 and Table 3.3). The beam width increased with inserting the DM into the femtosecond laser chain, but that might have been caused by too large beam size at the DM entrance pupil (Table 3.3). Still, we saw some higher order aberrations in the focus.

Measurement	W_x (mm)	W_y (mm)	M_x^2	M_y^2	z_{0x} (mm)	z_{0y} (mm)
Laser only	0.034	0.039	1.14	1.34	217.7	219.9
DM loop	0.049	0.043	1.36	1.22	220.0	219.9

TABLE 3.3: Measurements with the deformable mirror in the compressor

Conclusion

All optical systems have imperfections, which cause disturbances in the wavefront of the beam. These so called optical aberrations are almost always undesirable, because they reduce the properties of the light propagating through the system. This makes aberrated systems inefficient. For example, laser cutting technologies depend on the focused beam size (cut size) and beam intensity (cut depth) etc.

The aim of this thesis was to implement a cost efficient deformable mirror into a femtosecond laser chain, in order to reduce aberrations in the femtosecond laser beam. The Thorlabs deformable mirror has a custom-made ultrafast coating, which reduces the risk of damage to the mirror due to high beam intensities in femtosecond lasers. Femtosecond lasers are very common not only in research laboratories, but are also used in many industrial and medical applications. Currently available methods for reducing aberrations in high-intensity laser beams are expensive, thus make this project a promising alternative.

This thesis gave an overview of optical aberrations, Zernike polynomials, and adaptive optics. We used three methods for measurements: a setup with a HeNe laser, a setup with an uncompressed femtosecond laser beam and a setup of a femtosecond laser with the deformable mirror implemented into the chain. We took measurements of the focus with a camera and of the wavefront aberrations with the Thorlabs Shack-Hartmann wavefront sensor. The measurements were divided into stages. Firstly, we measured original beams of the laser, secondly, inserted flat deformable mirror into the chain, thirdly, started the loop program if possible (not with the deformable mirror in the compressor) and finally, used manual mirror surface control for the last two measurements .

The research work performed in this thesis resulted in the following findings. We learned that the deformable mirror caused rather strong aberrations (mainly astigmatism) in all the setups, which means that placing the mirror into the setup prevents the usage of the setup without the loop or manual control. We also saw that in order to avoid unwanted reflections from the sidearms, the beam must correspond to the deformable mirror's pupil size. The provided loop program is suitable for reducing lower-order aberrations. In addition, some of the mirror segments are overcompensating without causing a noticeable change in the lower-order Zernike coefficients, but causing many higher-order aberrations. This means that even though the corrected beam had almost no lower-order aberrations, higher-order aberrations were added, producing reduced focusability and peak intensity of the beam. This raised the need for manual control of the deformable mirror shape. Manually controlling the deformable mirror enabled a slightly improved focusability and wavefront of the beam. This showed that even a small change in the deformable mirror shape could affect the beam's parameters considerably. Integrating the deformable mirror into the femtosecond laser chain we saw that the astigmatism of the beam could be

reduced considerably, however the overall beam quality decreased slightly. This was probably caused by the higher-order aberrations introduced by the deformable mirror.

To summarise, the Thorlabs deformable mirror is a cost-effective adaptive optics solution that can be integrated into a femtosecond laser chain without damage, when the mirror is placed before the compressor to reduce peak intensity. Aberrations to the laser beam, which are a result of all optical components in the laser, can be corrected to a certain degree. Whereas lower-order aberrations can be corrected, the deformable mirror itself introduces higher-order aberrations, which most likely result from complicated undesired deformations of the mirror membrane, which do not correspond to any Zernike order. Even though we did not overall achieve enhanced beam quality, further measurements could be done by writing a specialized loop program for the femtosecond laser chain corrections. The potential benefits of using the Thorlabs custom-coated deformable mirror to correct the output of the femtosecond laser are evident.

Outlook

The deformable mirror used in this thesis shows great promise for wavefront correction in femtosecond lasers. However, the results of this thesis showed that this specific deformable mirror could not be implemented to enhance the focused intensity of the femtosecond laser's output. We were not able to use the loop program in order to correct the aberrations, because of the restrictions of the adaptive optics system, and the loop program. We saw from the measurements that manually controlling the deformable mirror would improve the results. Subsequently, one could attempt to write its own program for the loop control in order to make the system more flexible. The program should be able to measure aberrations at the femtosecond laser output and implement the measurements to a special loop program. In this way, the wavefront aberrations could be measured in the output of the laser and corrected by the deformable mirror before compression. All in all, this project has a promising prospect.

Bibliography

[1] D. Strickland and G. Mourou. Compression of amplified chirped optical pulses. *Optical Communications*, 56(3):219–221, 1985. URL http://www.sciencedirect.com/science/article/pii/0030401885901208.

[2] A. E. Siegman. How to (maybe) measure laser beam quality. In *DPSS (Diode Pumped Solid State) Lasers: Applications and Issues*. Optical Society of America, 1998. URL http://www.opticsinfobase.org/abstract.cfm?URI=DLAI-1998-MQ1.

[3] D. Malacara-Hernández and Z. Malacara-Hernández. *Handbook of Optical Design*. CRC Press, 3rd edition, 2013.

[4] M. Laan. Lecture notes on aberrations. http://www.physic.ut.ee/instituudid/efti/loengumaterjalid/opt/optika/geoopt/GO3/pt3.htm. Accessed: 2015-04-14.

[5] F. Trager, editor. *Springer Handbook of Lasers and Optics*. Springer, 2nd edition, 2012.

[6] Thorlabs. WFS series operation manual. http://www.thorlabs.de/thorcat/19900/WFS150-5C-Manual.pdf, 2012.

[7] J. Y. Wang and D. E. Silva. Wave-front interpretation with Zernike polynomials. *Applied optics*, 19(9):1510–8, 1980. URL http://www.ncbi.nlm.nih.gov/pubmed/20221066.

[8] M. Born and E. Wolf. *Principles of Optics - Electromagnetic Theory of Propagation, Interference and Diffraction of Light*. Cambridge University Press, 7th edition, 2005.

[9] V. N. Mahajan and J. A. Diaz. Imaging characteristics of Zernike and annular polynomial aberrations. *Applied Optics*, 52(10), April 2013.

[10] V.N. Mahajan. *Optical Imaging and Aberrations, Part III: Wavefront Analysis*. SPIE Press, 2013.

[11] J.W. Goodman. *Introduction to Fourier Optics*. The McGraw-Hill Companies, Inc., 2nd edition, 1996.

[12] Introduction to gaussian beam optics. http://fp.optics.arizona.edu/opti471B/Reading/lab4/MG_GBO_Tutorial.pdf. Accessed: 2015-06-01.

[13] R. K. Tyson. *Introduction to Adaptive Optics*. SPIE Publications, 2000.

[14] P.-Y. Madec. Overview of deformable mirror technologies for adaptive optics and astronomy, 2012. URL `http://dx.doi.org/10.1117/12.924892`.

[15] Wikipedia – deformable mirror. `https://en.wikipedia.org/wiki/Deformable_mirror`. Accessed: 2015-06-01.

[16] E. Hecht. *Optics*. Addison-Wesley, 4th edition, 2001.

[17] C.R. Nave. Hyperphysics - helium-neon laser. `http://hyperphysics.phy-astr.gsu.edu/hbase/optmod/lasgas.html`, 2012.

[18] D. Guenot. *Probing Electron Correlation on the Attosecond Timescale*. Phd thesis, Lund University, 2014.

[19] E. Witting Larsen. Generation of tunable broadband deep ultraviolet radiation from gaseous media using ultrashort laser pulses. Diploma thesis, Aarhus University and Lund University, 2011.

[20] Miranda M. Persson A. L'Huillier A. Fordell, T. Envelope phase stabilization of a multi-millijoule, regenerative-amplifier-based chirped-pulse amplifier system. *Optics Express*, 17(23), November 2009.

[21] Thorlabs. DMP40 operation manual. `http://www.thorlabs.de/thorcat/MTN/DMP40_M-P01-Manual.pdf`, 2014.